

Reply to interactive comments on “Evaluating Trends and Seasonality in Modeled PM_{2.5} Concentrations Using Empirical Mode Decomposition”

Anonymous Referee #3

This manuscript presented an evaluation of the WRF-CAMQ model simulated temporal trends through a detailed comparison with observation using improved CEEMDAN method. The comparison was based on measurements of PM_{2.5} and its key components, i.e., sulphate, nitrate, ammonium, chloride, organic carbon, and elemental carbon, made at three ground monitoring stations in US from t 2002 to 2008. It is clearly demonstrated that the improved CEEMDAN approach can decompose the observed and simulated temporal trends, which allows to extract more information from the comparisons of individual temporal modes. For example, the authors concluded that the model can better simulate the rate of change of the multi-year trend than the absolute magnitude. At the same time, model can generally reproduce the amplitudes of the sub-seasonal and annual variations for PM_{2.5}, sulphate, and OC. This study revealed that it appears there is a temporal phased shift between the observed and model simulated PM_{2.5}, OC, and EC as large as a half year. It is further suggested that this phase shift indicated “a need for proper temporal allocation of emissions”. In general, the manuscript is well organized.

We thank the reviewer for the positive assessment of our manuscript and for providing constructive feedback to help improve the quality of the manuscript. We have addressed all questions and suggestions in our response as well as in the text or figures, as necessary. Please see detailed responses below and the marked-up version of the revised manuscript.

This reviewer believes that this is an important work which can potentially help identifying model deficiencies. However, there several concerns needed to be addressed:

- 1) The authors correctly stated that EMD is a widely used methodology in various field. At the same time, this reviewer would like to suggest that the authors should consider adding some brief high-level descriptions of the method. This will improve the manuscript’s readability, especially for those who are not familiar with EMD methods. It is also important to clearly state the criteria how the modes are determined and separated. The statement in line 134-135, “to achieve best mode separation”, leaves much room for interpretation. The discussion on determination of t_p and t_m is interesting and thorough. It does, however, leave an impression that the evaluation of t_p and t_m is somewhat uncertain and is not completely deterministic. This reviewer would like to suggest adding additional text to discuss if the determination of t_p and t_m is sufficiently accurate or useful for model assessment to identify issues in the processes at the similar time scale as decomposed t_p and/or t_m . This will strengthen the manuscript to demonstrate the usefulness of the improved CEEMDAN approach in model assessments.

The decomposition process and parameters controlling the decomposition have been added in Section 3.1 as suggested. The “best mode separation” is also further explained following the reviewer’s suggestion.

CEEMDAN is a technique that is particularly suitable to analyze non-linear and non-stationary time series data. The decomposed time series of speciated and total PM_{2.5} reveal the agreement/disagreement between observations and model simulations at various intrinsic temporal scales without any predetermined assumptions on the data. Both t_p and t_m represent approximate estimates of the characteristic scale of an IMF, where non-linear and non-stationary processes with close temporal scales could exist. For t_p (from the revised text): “The peak estimates can be biased if more than one high-power frequency is located closely within one IMF. Thus, the power spectrum and t_p is only used as a fast screening tool to determine if a desired decomposition is accomplished.” For t_m : “As the frequency decreases, the mean period estimates become less accurate because of the limited time span compared with the length of the cycle and should be carefully interpreted.” We have added the following test in Section 4.1: “Since each IMF represents a non-stationary process, the mean period t_m is only an estimate of its characteristic scale. Evaluation of t_m might not necessarily be able to identify issues with corresponding model simulations, and it does not indicate any information on the magnitude or the phase of the time series, which is more important and will be further discussed in Sections 4.3 to 4.4.”.

- 2) Section 2 (starting from line 74) provided a good discussion on how the observation data sets are selected. It is equally important to discuss the temporal resolution of model in terms of the driving factors, e.g., emissions. This will give readers a sense if one should expect if the model should reproduce observations at certain temporal scale. For example, if the emissions are given in yearly average, one would consider the impact of the lack emission temporal variability on the comparison of seasonal and/or sub-seasonal trends.

We added the following text in Section 2: “Annual emissions for the CMAQ simulations were estimated using the methodology described in Xing et al. (2013). Briefly, the National Emissions Inventory (NEI) for 1990, 1995, 1996, 1999, 2001, 2002 and 2005 and a number of sector-specific long-term databases containing information about trends in activity data and emission controls were used to create county-level annual emissions for a total of 49 emission sectors. Prior to being used as input to the CMAQ simulations, these annual emissions were then temporally and spatially allocated to provide hourly emissions based on monthly, weekly, and diurnal temporal cross-reference and profile data from the 2005 NEI modeling platform. These profile data vary by emissions source and sometimes by state and county and are generally based on surveys and extrapolation of activity data which can be subject to uncertainty. Exceptions to the use of 2005 NEI platform temporal profile data for temporal allocation were emissions from electric generating units (EGU) which directly used measured hourly emissions after 1995 and wildfire emissions that used climatological monthly, weekly, and diurnal profiles for temporal allocation.”

The large discrepancy in the magnitude of some long-term trend component seen in Fig. 6 is likely pointing to the systematic bias in the annual emission estimations as discussed in Xing et al. (2013): “...since this study mainly focused on trends rather than the absolute value in each individual year, some sectors (e.g., industrial processes) and sub-sectors (types of combustion and stoves) may not have been well considered or examined.” The intra-annual emission allocation could possibly impact the model performance at the seasonal and sub-seasonal scales. This discussion of the impact of emissions on the long-term trend has been added in Section 4.2.

- 3) This reviewer believes that the concluding remark of “indicating the need for proper allocation of emissions” is an important conclusion. However, it was not adequately justified. There are many controlling factors and processes. The authors should have provided more discussions to illustrate how they narrowed to emissions as the likely factor. It should also be pointed out that SOA is typically a large component of OC. Changes in emissions to affect OC will likely have implications on O3.

We would like to clarify that our illustrative application of the new methodology to PM_{2.5} time series at three specific sites does not allow us to conclude that errors in the temporal allocation of PM emissions are the controlling factors for disagreements between observed and modeled annual cycle. While we believe that they do play a role as discussed below, we also know that the CMAQ version used for these simulations has underestimated the formation of SOA, which would also affect the modeled annual cycle of OC (e.g. Appel et al., 2017; Murphy et al., 2017; Xu et al., 2018). Because of the underestimation of SOA, OC in the simulations analyzed here has an overestimated relative contribution of primary OC which, in turn, makes its temporal variations analyzed by CEEMDAN sensitive to the temporal allocation of primary PM and specifically primary OC emissions. The full statement partially quoted by the reviewer points to both factors “indicating the need for proper allocation of emissions and an updated treatment of organic aerosols compared to the earlier model version used in this set of model simulations”. Without running a new set of decadal simulations with a newer version of the model and/or modified temporal allocation of emissions, we are unable to determine the relative importance of these factors at the sites examined. However, if such simulations were to be performed in the future, the CEEMDAN methodology can help demonstrate the benefits of updated emissions allocations and/or the SOA process representation.

- 4) The authors presented detailed trend analysis on PM_{2.5} and its components. It is also scientifically interesting to understand the relative contribution of each component and their contribution to the identified temporal variability, which are useful to gain insights into controlling factors. This reviewer would like to suggest the authors to consider addition of the trend analysis on the relative contribution of sulphate, nitrate, ammonium,

organic carbon, and elemental carbon to PM_{2.5}. More specific to the manuscript, it would be much easier to interpret the results shown in Table 1, 2, and 3 if the relative contribution of each component is known.

Yes, it would be useful to explicitly show the importance of each component in driving the trend of total PM_{2.5} in both observations and model simulations. The time series of the concentration share of each component (e.g. OC/Total PM_{2.5} %) is added in Fig. S6 in the supplement. However, the decomposition of the concentration share is not included since there is not much change in the percentage share in its trend component (few percentages at most in very limited cases) and the ratio does not necessarily have strong seasonality because of the phase difference in specific component and total PM_{2.5}. Thus, including the trend component of time variant share of the ratio would only complicate the interpretation of the results. Instead, we have added a new Table 1 (see below) to show the overall concentration share of each component for both observations and model simulations to reflect the relative importance of different species.

Table 1. Concentration share (%) of different components in total PM_{2.5}. It is estimated by dividing the mean trend components of each species by that of total PM_{2.5} for both OBS and CMAQ, multiplied by 100. The concentration share of the remainder species (*Rem*) is estimated by subtracting all the available species share from 100 to compensate for the small discrepancies caused by the rounding up process and uncertainty in the mode decomposition. “-” indicates the data is not available (same applies for all other tables).

		SO ₄	NO ₃	NH ₄	OC	EC	Cl	Rem
QURE	OBS	38	7	–	19	5	1	30
	CMAQ	19	15	–	14	5	1	47
RENO	OBS	7	13	5	46	11	–	20
	CMAQ	11	4	2	30	7	–	45
ATL	OBS	28	6	10	24	8	–	24
	CMAQ	22	10	8	17	9	–	33

- 5) In general, model evaluation is designed to improve model. It is difficult to relate the comparison results presented in this manuscript to specific model deficiencies in description of the chemical/physical processes and/or issues in model data sets, meteorological field and/or emission data. As sulphate, OC, nitrate are controlled by very different chemical processes, this reviewer would like to encourage the authors to further explore the difference in the comparison results for these species, which may reveal additional insights into the process-level model deficiencies.

We thank the reviewer for recognizing the potential of the proposed methodology in helping identify problems in the specific processes and/or model input. However, without running a new set of decadal simulations with a newer version of the model and/or

modified temporal allocation of emissions, we cannot determine specific model deficiencies and/or issues in the model input data sets.

Specific Comments:

- 1) Figure 3 is hard to read because of log-log scale. It may be better to change the x-axis to the IMF number and y-axis to the ratio between model and observation characteristic scales. A second y-axis can be added to show the absolute characteristic scales for each IMF.

We thank the reviewer for the suggestion. However, because of the large discrepancies in the scales of IMFs (few days to thousands of days), log scale has to be employed to show the scales for all IMFs. Given that the characteristic periods are not easy to read from the plot, we provided the average characteristic periods for sub-seasonal and seasonal IMFs in the text. Moreover, since “not all IMFs from observation are being simulated and vice versa”, a figure is needed for each site to show the characteristic scales (at least for the last few IMFs) separately for observations and model simulations. Thus, we have moved the inlet figures to Figure 3d-f for clarity and added the explanation in the caption. Adding a second y-axis and showing only observed characteristic scale would result in a very busy plot and we will not be able to achieve the second point above. Please find our revision to the figure in the manuscript and below.

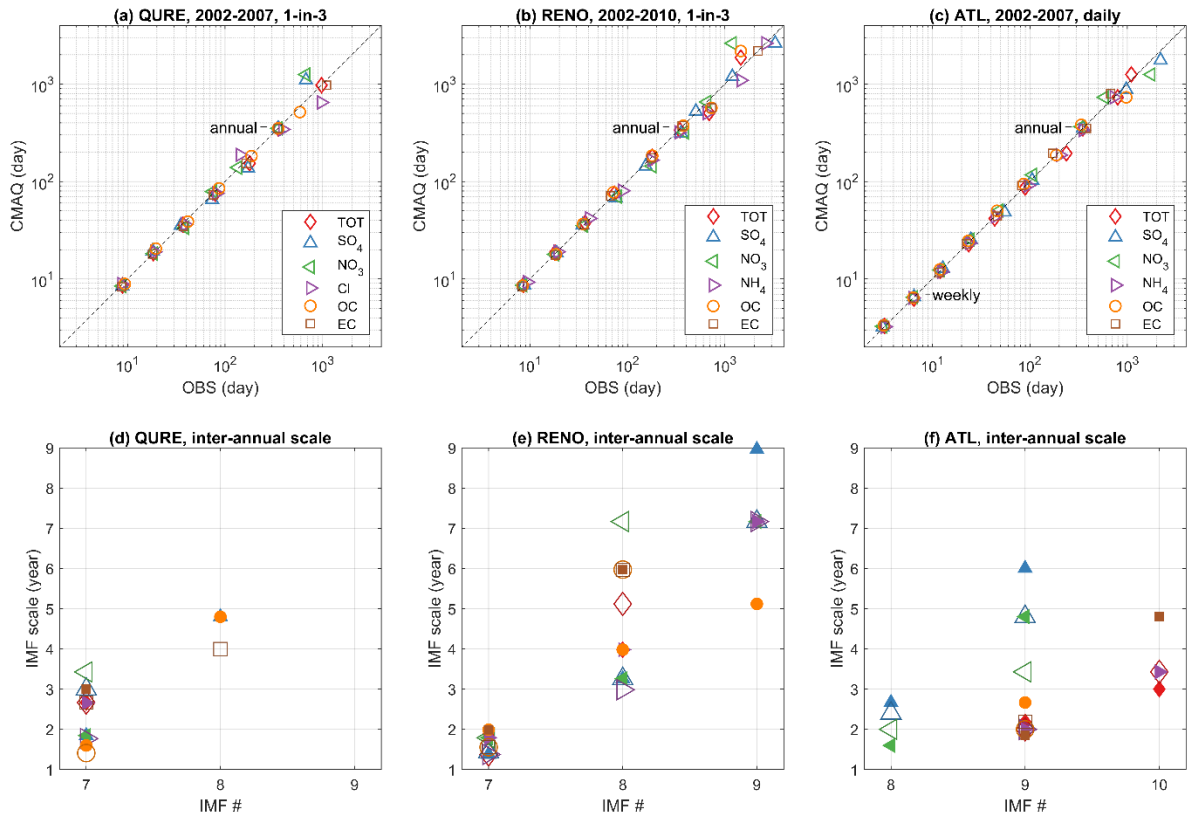


Fig. 3. The characteristic scales (t_m) resolved in the IMFs of observed and simulated total and speciated PM_{2.5} for (a, d) QURE, (b, e) RENO and (c, f) ATL. In (a-c), IMF1 to the last pair of IMFs with increasing characteristic periods are shown from bottom left to top right. Mean periods of IMFs with scales longer than a year are being displayed in (d-f) with the same shapes as in the legend above to show the characteristic scales of all decomposed IMFs given that not all IMFs from observation are being simulated and vice versa. In the (d-f), species decomposed from observations are shown with smaller filled shapes, while species decomposed from simulations are represented by larger open shapes in slightly darker shades.

- 2) Section 4.2. Figure 6 shows some variation in time-derivatives. At the same, this reviewer would like to argue that about half of cases shown in the figure can be well approximated by linear assumption. The authors should comment on this aspect.

Linear assumption is useful in many cases, and linear trends do provide a general idea of magnitude of the change as well as whether the linear trend is significant or not. EMD is particularly useful for analyzing meteorological and pollutant time series, which are non-linear and non-stationary. The decomposed trend components can provide the exact time span and magnitude of a decreasing/increasing change throughout time. If we take the trend component of observed OC at ATL as an example, the OC level is stable at around 4.5 $\mu\text{g}/\text{m}^3$ in 2002 and 2003 and decreases at varying rates during 2004-2007.

Anonymous Referee #4

General Comments: This paper introduces a new approach for process-based model evaluation of speciated PM_{2.5}, which allows for the assessment of the performance of regional-scale air quality models like CMAQ on the intrinsic time-dependent longterm trend and cyclic variations in daily average PM_{2.5} and its species. The authors tested the method with time series data at three sites. The data are generally sound, whereas some results and discussions of the study are still lack of persuasion.

One major concern is about how well the current approach's performance is compared with the previously published methods and some over-interpreted conclusions. The other is that it is not sure that the difference between the model and the new approach evaluation results can be simply explained by the inadequate description of nitrate or organics in the model. As the authors noted, they obtained abnormally low correlations of synoptic scale NO₃ at ATL and calls for a better representation of nitrate partitioning and chemistry. What about the results for the other two sites? The authors need to provide more information on such issues to make the conclusion robust.

We appreciate the time and effort devoted by the reviewer to provide suggestions that helped improve the quality of our paper.

Our temporal decomposition approach applied to PM_{2.5} and its speciated components is not directly comparable with the other approaches reported in the literature. To avoid any over-interpretation of the analyses, we have refrained from exploiting model performance on the characteristic time scales and have carefully aligned our interpretation with IMFs that are statistically significant (almost all seasonal cycles are statistically significant from noise as shown in Fig. S5). Also, the differences between observed and simulated total and speciated PM_{2.5} are driven by several factors discussed in the paper. We cannot conclude exclusively that there is inadequate description of nitrate or organics in the model. Other potential issues such as the improper allocation of emissions also contributed to the difference between model simulations and observations. To be specific, description of secondary organic matter formation and magnitude and variation of primary sources are emerging areas of research; NO₃ formation pathways are likely inadequately represented in the employed model version, and its predictions are also strongly influenced by the uncertainties in NH₃ emissions.

CMAQ fails to simulate the magnitude of NO₃ at all three sites with very abnormal r_{IMFn} . Moreover, NO₃ is the only component that has low correlation on the synoptic scale at ATL. The poor performance for NO₃ mentioned above at all three sites calls for the modeler to look at the representation of nitrate partitioning and chemistry as summarized in the conclusions: "The consistent large under/over-prediction of NO₃ variability at all temporal scales and magnitude in the trend component, as well as the abnormally low correlations on the synoptic scale NO₃ at ATL, calls for better representation of nitrate partitioning and chemistry."

Specific comments:

1. Introduction: “Evaluation of ten-year averaged monthly mean of PM2.5 simulated with WRF/Chem ...” how does the model performance of PM2.5 compositions simulation should also be summarized to provide an intact view on the previous results.

Unfortunately, Yahya et al. (2016) only compared the overall 10-year average of the PM compositions (sulfate, ammonium, nitrate, EC, and total carbon) from ground-based observations to that of the model simulations as the background map. Thus, we are not able to make any conclusions on the seasonality of PM2.5 components.

2. Line 36: “and other natural species...” what do natural species refer to?

Natural species refer to PM2.5 non-anthropogenic components such as crustal material. We have changed this to “crustal elements” in the revised manuscript to avoid confusion.

3. Line 47: “monthly or seasonal means” means of speciated PM2.5?

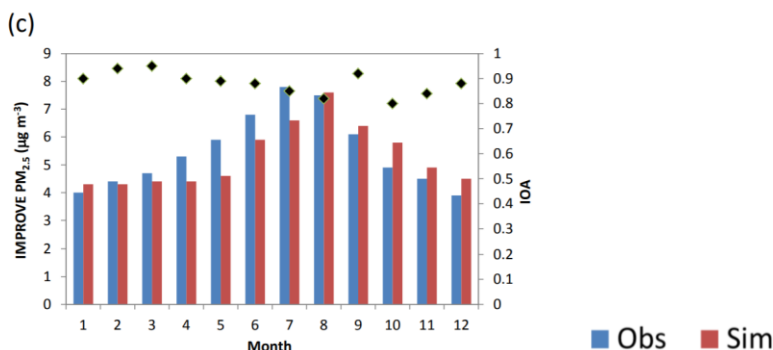
The sentence is rephrased as: “monthly or seasonal means of total and/or speciated PM2.5.”

4. Line 48: what do you mean by “ten-year averaged monthly mean”?

It is the monthly mean averaged over a period of ten years: ten-year averaged mean for Jan., Feb., ...

5. Line 51: “with a phase shift of few months” please explain phase shift.

The phase shift refers to that in Fig. 4c (copied below) in Yahya et al. (2016). The definition is similar to what we used in the evaluation of the cyclic signals: “the phase shift of an IMF n is defined as the days an IMF decomposed from modeled time series has to be shifted to maximize the correlation (R_{max}) with the corresponding IMF from observed PM2.5 time series.”



6. Line 55-57: "...long-term trends or interannual variations driven by climate change, emission control policies or other slow varying processes..." what is the main reason? Are there any previous results?

Changes in air quality concentrations, such as PM_{2.5}, are driven by changes in emissions and meteorological processes which highly impact the transport, chemical reactions and deposition of air pollutants. Thus, long-term trends reflect the impact of long-term changes in emissions (they might be governed by local control policies on anthropogenic emissions or climate-impacted natural emissions), long-term meteorological conditions (climate) and other slow varying processes (e.g. ENSO). There is no "main reason" among them. Here, we are simply stating that averaging over very long time periods can conceal signals driven by slow-changing processes: *"In addition, averaging of those monthly or seasonal means across multiple years may conceal the long-term trends or interannual variations driven by climate change, emission control policies or other slow varying processes."* We are not certain what the reviewer's query is directed at. Thus, we have left the sentence unaltered.

7. Line 68-74: I do not think this paragraph is necessary for the manuscript.

Following the reviewer's suggestion, the paragraph has been deleted in the revised manuscript.

8. Line 311: "RENO is located close to the border with California and is affected by large wildfire breakouts in the western U.S...." Is there any evidence for this demonstration?

The location of Reno, NV and the impact of California fire on July 10, 2008 is illustrated in Figure 1 (copied below) from Gyawali et al. (2009). We have also demonstrated the impact of 2008 fire season earlier in Section 4.1: *"The small variation in the estimated characteristic period of IMF6 is because this monitoring site is located in a wildfire prone region on the border of Nevada and California. Clear evidence can be seen from Fig. 4a that an extra annual cycle in the IMF6 of observations in the summer of 2008 is depicted, which is very possibly driven by the 2008 California Wildfires spanning from May until November."*

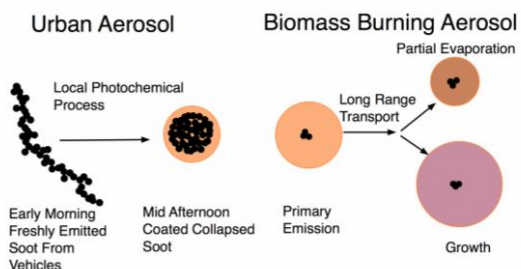


Fig. 1. Upper panel: Satellite image of smoke extending from northern California to Reno, Nevada on 10 July 2008. The smoke sources and wind trajectory were similar for much of July. Below panel: Conceptual model of emission and aging of urban and biomass burning aerosol.

9. Line 327-: “To sum up, the long-term trend at QURE is well simulated by the model.” This is unlikely consistent with the data presented in Table 1.

Our statement is based on the fact that the model has captured the decrease (i.e., rate of change), even though the absolute magnitude of the trend/long-term component is overestimated (which is what is shown in Table 1-now Table 2). We have re-phrased the sentence to: “To sum up, the decreasing long-term trend at QURE is well simulated by the model.”

10. Lines 333-335: “Species other than those in the available dataset may also play a considerable role in driving the agreements or disagreements between model simulations and observations of total PM2.5” What are the contribution of these species to PM2.5 at the studied sites?

We have decomposed the remaining components (*Rem*) and added an 8th line of figures for the trend component in *Rem* in Fig. 6. The overall concentration share (%) of the remaining components can be found in the newly added Table 1. We have also added Figure S6 in the supplement that shows time series of the concentration share of each component (e.g. OC/Total PM2.5 %).

11. Lines 367-368: “Both observed and simulated annual cycles at the RENO site are largely contaminated by the extreme events lasting for several months that are not properly simulated” is it possible to remove the data of extreme events before simulation, in order to eliminate the contamination?

These extreme events are very likely caused by large wildfires. We can eliminate emissions from wildfires in model simulations, but there is no straightforward way to eliminate contributions of wildfires in the observations. Thus, we kept the original observations and CMAQ model simulations, which included wildfire emissions.

12. Lines 384-387: “Specifically, the anti-correlation likely points to an inaccurate representation of the seasonal variation of the non-carbonaceous portion of organic matter due to an improper representation of organic aerosols in the model version analyzed here; this problem has since been corrected in more recent releases of the CMAQ model.” This sentence needs to be rewritten for clearance. And what does the noncarbonaceous portion of organic matter refer to?

The long sentence has been revised for clarity: *“Specifically, the anti-correlation likely points to an inaccurate representation of the seasonal variation of the non-carbonaceous portion of organic matter due to an incomplete representation of organic aerosols in the model version analyzed here; newer versions of the CMAQ model include updated treatment of organic aerosols (e.g., additional SOA formation pathways, improvements in representation of primary OM emissions) which is likely to correct the mentioned features (Appel et al., 2017; Murphy et al., 2017; Xu et al., 2018).”*

The non-carbonaceous portion of organic matter refers to the portion of organic matter consisting of oxygen, hydrogen, and nitrogen.

Minor:

13. Line 17: “chloride (Cl) organic”

Corrected.

14. Line 311: “U.S. as can been seen”

Corrected.

1
2
3
4
5
6
7
8
9
10
11
12
13
14
15
16
17
18
19
20
21
22
23
24
25
26
27
28
29
30

Evaluating Trends and Seasonality in Modeled PM_{2.5} Concentrations Using Empirical Mode Decomposition

Huiying Luo¹, Marina Astitha^{1*}, Christian Hogrefe², Rohit Mathur², S. Trivikrama Rao^{1,3}

¹University of Connecticut, Department of Civil and Environmental Engineering, Storrs-Mansfield, CT, USA

²U.S. Environmental Protection Agency, Research Triangle Park, NC, USA

³North Carolina State University, Raleigh, NC, USA

*Corresponding author: Marina Astitha, Civil and Environmental Engineering, University of Connecticut, 261 Glenbrook Road, Storrs, CT, 06269-3037, Phone: 860-486-3941, Fax: 860-486-2298, Email: marina.astitha@uconn.edu.

Abstract. Regional-scale air quality models are being used for studying the sources, composition, transport, transformation, and deposition of fine particulate matter (PM_{2.5}). The availability of decadal air quality simulations provides a unique opportunity to explore sophisticated model evaluation techniques rather than relying solely on traditional operational evaluations. In this study, we propose a new approach for process-based model evaluation of speciated PM_{2.5} using improved Complete Ensemble Empirical Mode Decomposition with Adaptive Noise (improved CEEMDAN) to assess how well version 5.0.2 of the coupled Weather Research and Forecasting model - Community Multiscale Air Quality model (WRF-CMAQ) simulates the time-dependent long-term trend and cyclical variations in the daily average PM_{2.5} and its species, including sulfate (SO₄), nitrate (NO₃), ammonium (NH₄), chloride (Cl₂), organic carbon (OC) and elemental carbon (EC). The utility of the proposed approach for model evaluation is demonstrated using PM_{2.5} data at three monitoring locations. At these locations, the model is generally more capable of simulating the rate of change in the long-term trend component than its absolute magnitude. Amplitudes of the sub-seasonal and annual cycles of total PM_{2.5}, SO₄ and OC are well reproduced. However, the time-dependent phase difference in the annual cycles for total PM_{2.5}, OC and EC reveal a phase shift of up to half year, indicating the need for proper temporal allocation of emissions and for updating the treatment of organic aerosols compared to the model version used for this set of simulations. Evaluation of sub-seasonal and inter-annual variations indicates that CMAQ is more capable of replicating the sub-seasonal cycles than inter-annual variations in magnitude and phase.

Keywords

Model evaluation, coupled WRF-CMAQ, improved Complete Ensemble Empirical Mode Decomposition (EMD) with Adaptive Noise, Speciated PM_{2.5}, Scale Separation, Seasonality, Trend

31 **1 Introduction**

32 It is well recognized that inhalable fine particulate matter (PM_{2.5}) adversely impacts human health and the
33 environment. Regional-scale air quality models are being used in health impact studies and decision-making related
34 to PM_{2.5}. Long-term model simulations of PM_{2.5} concentrations using regional air quality models are essential to
35 identify long-term trends and cyclical variations such as annual cycles in areas larger than what is covered by in-situ
36 measurements. However, total PM_{2.5} concentrations are challenging to predict because of the dependence on the
37 contributions from individual PM_{2.5} components, such as sulfates, nitrates, carbonaceous species, and ~~other natural~~
38 ~~species~~crustal elements. In this context, a detailed process-based evaluation of the simulated speciated PM_{2.5} must be
39 carried out to ensure acceptable replication of observations so model users can have confidence in using regional air
40 quality models for policy-making. Furthermore, ~~process-based~~process-based information can be useful for making
41 improvements to the model.

42 Some of the trend or step change evaluations of regional air quality models in the past have focused on specific pairs
43 of years (Kang et al., 2013; Zhou et al., 2013; Foley et al., 2015). These studies do not properly account for the sub-
44 seasonal and inter-annual variations between those specific periods. Trend evaluation is commonly done by linear
45 regression of indexes such as the annual mean or specific percentiles, assuming linearity and stationarity of time series
46 (Civerolo et al., 2010; Hogrefe et al., 2011; Banzhaf et al., 2015; Astitha et al., 2017). The problem with the linear
47 trend evaluation is that there is no guarantee the trend is actually linear during the period of the study because the
48 underlying processes are in fact nonlinear and nonstationary (Wu et al., 2007).

49 Seasonal variations are usually studied and evaluated by investigating the monthly or seasonal means of total and/or
50 speciated PM_{2.5} (Civerolo et al., 2010; Banzhaf et al., 2015; Yahya et al., 2016; Henneman et al., 2017). Evaluation of
51 ten-year averaged monthly mean (i.e., ten-year averaged mean in Jan., ..., Dec.) of PM_{2.5} simulated with WRF/Chem
52 against the Interagency Monitoring of Protected Visual Environments (IMPROVE) by Yahya et al. (2016) shows that
53 the model captures the observed features of summer peaks in PM_{2.5} with a phase shift of few months. However,
54 according to the analysis (Fig. 10) in Henneman et al. (2017), the seasonality shown in monthly-averaged PM_{2.5} time
55 series is much less distinguishable compared with that of ozone and CMAQ (version 5.0.2) does not replicate the
56 monthly PM_{2.5} quite well with large underestimation in the summer months. In these studies, the seasonality might not
57 be well represented by the preselected averaging window size of one or three months. In addition, averaging of those
58 monthly or seasonal means across multiple years may conceal the long-term trends or interannual variations driven
59 by climate change, emission control policies or other slow varying processes.

60 To address the above-mentioned problems, we propose a new method for conducting air quality model evaluation for
61 PM_{2.5} using improved CEEMDAN. Improved CEEMDAN is an Empirical Mode Decomposition (EMD)-based, data-
62 driven intrinsic mode decomposition technique that can adaptively and recursively decompose a nonlinear and
63 nonstationary signal into multiple modes called intrinsic mode functions (IMFs) and a residual (trend component)
64 (Huang et al., 1998; Wu and Huang, 2009; Yeh et al., 2010; Torres et al., 2011; Colominas et al., 2014). It does not
65 require any preselection of the temporal scales or assumptions of linearity and stationarity for the data, thereby
66 providing some insights into time series of PM_{2.5} concentrations and its components. Decomposed PM_{2.5} long-term

67 trend components and annual cycles from observed and simulated $PM_{2.5}$ serve as the intuitive carrier of the trend and
68 seasonality evaluation. In the meantime, several other IMFs with characteristic time scales ranging from multiple days
69 to years are also decomposed, enabling model evaluation of the less studied sub-seasonal and inter-annual variations.

70 ~~Section 2 describes the coupled WRF-CMAQ model simulations and corresponding observations from multiple~~
71 ~~speciated $PM_{2.5}$ networks. Section 3 presents an overview of the EMD and improved CEEMDAN technique and the~~
72 ~~statistical metrics accompanying model evaluation, including the time dependent intrinsic correlation (TDIC) on the~~
73 ~~decomposed IMFs (Chen et al., 2010; Huang and Schmitt, 2014; Derot et al., 2016). Section 4 describes the findings~~
74 ~~on the long term trend and seasonality in total $PM_{2.5}$ and its components, as resolved by the improved CEEMDAN~~
75 ~~technique and includes a discussion on the sub-seasonal, seasonal, and inter-annual variability. The conclusions from~~
76 ~~this work are presented in section 5.~~

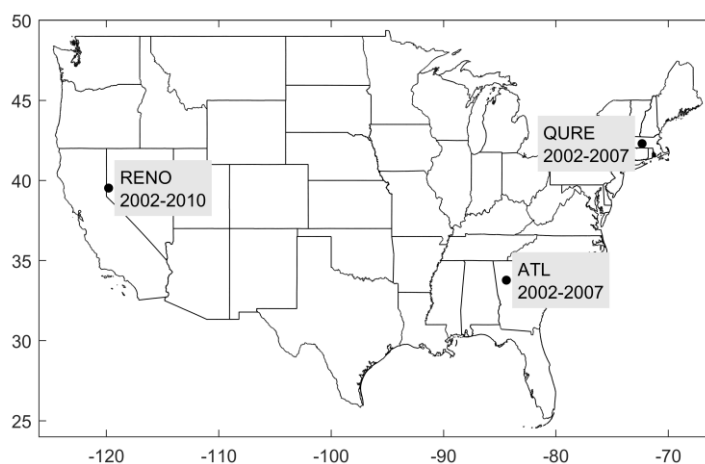
77 **2 Coupled WRF-CMAQ $PM_{2.5}$ Simulations and Observations**

78 The two-way coupled WRF-CMAQ (version 5.0.2) is configured with a 36 km horizontal grid spacing over the
79 contiguous United States (CONUS) with 35 vertical layers of varying thickness extending from the surface to 50 mb
80 (Wong et al., 2012; Gan et al., 2015). Time-varying chemical lateral boundary conditions were derived from the 108
81 km resolution hemispheric WRF-CMAQ (Mathur et al., 2017) simulation for the 1990-2010 period (Xing et al., 2015).

82 The simulations are driven by a comprehensive emission dataset which includes ~~the~~ aerosol precursors and primary
83 particulate matter (Xing et al., 2013, 2015). Annual emissions for the CMAQ simulations were estimated using the
84 methodology described in Xing et al. (2013). Briefly, the National Emissions Inventory (NEI) for 1990, 1995, 1996,
85 1999, 2001, 2002 and 2005 and a number of sector-specific long-term databases containing information about trends
86 in activity data and emission controls were used to create county-level annual emissions for a total of 49 emission
87 sectors. Prior to being used as input to the CMAQ simulations, these annual emissions were then temporally and
88 spatially allocated to provide hourly emissions based on monthly, weekly, and diurnal temporal cross-reference and
89 profile data from the 2005 NEI modeling platform. These profile data vary by emissions source and sometimes by
90 state and county and are generally based on surveys and extrapolation of activity data which can be subject to
91 uncertainty. Exceptions to the use of 2005 NEI platform temporal profile data for temporal allocation were emissions
92 from electric generating units (EGU) which directly used measured hourly emissions after 1995 and wildfire emissions
93 that used climatological monthly, weekly, and diurnal profiles for temporal allocation. ~~The r~~eaders can refer to Gan
94 et al. (2015) for additional model information and the trend evaluation against seven pairs of sites from the CASTNET
95 (Clean Air Status and Trend Network) and IMPROVE networks for 1995-2010. We obtained the 2002-2010 daily
96 average $PM_{2.5}$ and its speciated time series from the set of simulations with direct aerosol feedback. The earlier years
97 of 1990-2001 are not included in this evaluation because of the limited availability of speciated $PM_{2.5}$ observations.

98 To avoid misinterpretation of data due to the presence of missing values, only sites with continuous complete long-
99 term record for total $PM_{2.5}$ and its speciation including SO_4 , NO_3 , NH_4 , OC, EC, and Cl are studied (Fig. 1). All of the
100 selected sites have data coverage above 90% each year for at least six consecutive years between 2002 and 2010
101 (equivalent to 30% for 1-in-3 days sampling sites). This strict data selection led to the sparsity of this type of

102 observations for the study period. QURE, a rural site carrying out 1-in-3 days sampling of total and speciated $PM_{2.5}$
 103 of SO_4 , NO_3 , OC, EC_7 and Cl, is located in Quabbin Summit, MA. It is one of the three sites from the IMPROVE
 104 network that has at least six continuous years of speciated observations and was selected here to demonstrate the
 105 application of the proposed method in rural areas. It should be noted that the majority of the observed Cl in 2002 and
 106 2003 is negative due to a filter issue problem which was not addressed until 2004 (White, 2008). Thus, simulations of
 107 Cl are only evaluated during 2004-2007 at this site. Station RENO, located in urban Reno, NV, is also a 1-in-3 days
 108 sampling site of total and speciated $PM_{2.5}$ of SO_4 , NO_3 , NH_4 , OC_7 and EC, and it is the only Chemical Speciation
 109 Network (CSN) site that fulfills this data coverage requirement. The third site ATL in the Southeastern Aerosol
 110 Research and Characterization Study (SEARCH) network is located 4.2 km northwest of downtown Atlanta, GA. It
 111 is the only long-term site available with daily sampling rate (Hansen et al., 2003; Edgerton et al., 2005) that meets the
 112 data coverage requirement. The best-estimate (BE), a calculated concentration intended to represent what is actually
 113 in the atmosphere (Edgerton et al., 2005), of the total $PM_{2.5}$ and SO_4 , NO_3 , NH_4 , and EC components are retrieved for
 114 the evaluation. OC component is a direct measurement. These three sites have a continuous record covering at least 6
 115 years (2002 – 2007 for QURE and ATL and 2002 – 2010 for RENO) that allows an evaluation of long-term trends.



116
 117 **Fig. 1. Location and data coverage of the $PM_{2.5}$ monitoring sites QURE, RENO and ATL.**

118 3 Methodology

119 3.1 Empirical Mode Decomposition

120 The Empirical Mode Decomposition (EMD) technique, proposed in the late 1990s, is capable of adaptively and
 121 recursively decomposing a signal into multiple modes called intrinsic mode functions (IMFs), where each mode has
 122 a characteristic frequency, and a residual with at most one extremum (Huang et al., 1998). EMD decomposes the
 123 original signal into several IMFs and a residual through a repeated process called “sifting”: first, local maxima and
 124 minima are identified and interpolated separately with a cubic spline as the upper and lower envelop; then an IMF
 125 candidate is derived by subtracting the mean of the envelopes from the original signal. If the candidate satisfies the
 126 following criteria (Huang et al., 1998), it is saved as the first IMF (IMF1), and the remaining portion (original signal

– IMF1) is treated as a new input signal for the decomposition of the remaining IMFs; otherwise, more sifting processes should be carried out until the candidate becomes an IMF.

1) The number of extrema (maxima and minima) and the number of zero-crossings must be equal or differ at most by one;

2) The local mean at any point, the mean of the envelope defined by local maxima and the envelope defined by local minima, must be zero.

In this way, IMF1, IMF2, ... are decomposed recursively with decreasing characteristic frequency. The final remaining residual (trend) could be a monotonic function of time or a long-term component with one extremum at most. The decomposed signal then is expressed as the summation of all IMFs and the final residual:

$$x = \sum_{i=1}^k d_i + r \quad (1)$$

where x is the original signal, d_i is the i^{th} IMF, k is the total number of the IMFs and r is the final residual. Each IMF has the following properties (Huang et al., 1998):

1) The number of extrema (maxima and minima) and the number of zero-crossings must be equal or differ at most by one;

2) The local mean at any point, the mean of the envelope defined by local maxima and the envelope defined by local minima, must be zero.

Nevertheless, “mode mixing”, where oscillations with very disparate scales can be present in one mode or vice versa, is commonly reported. To cope with this issue, multiple noise assisted EMD have been developed successively (Wu and Huang, 2009; Yeh et al., 2010; Torres et al., 2011; Colominas et al., 2014). It is evident that the latest improved Complete Ensemble EMD with Adaptive Noise (improved CEEMDAN) manages to alleviate the problem of mode mixing with the benefit of reducing the amount of noise presented and avoiding spurious modes (Colominas et al., 2014). Moreover, the end effects or boundary effects have been addressed by its predecessor EEMD (Ensemble Empirical Mode Decomposition) by extrapolating the maxima and minima, and behaved well in numerous time series with dramatically variant characteristics (Wu and Huang, 2009). The extrapolation of maxima and minima is proven to be more effective compared with the extrapolation of the signal itself such as repetition or reflection (Rato et al., 2008).

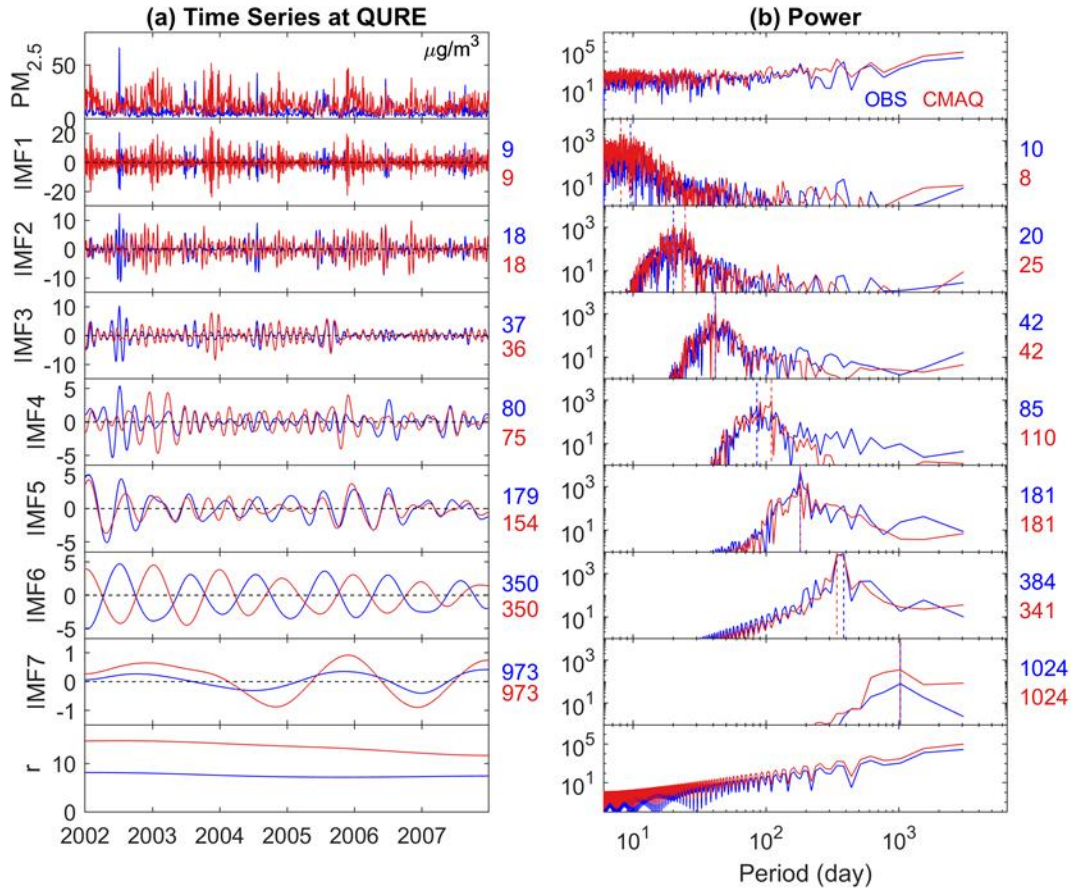
Given the EMD’s ability to deal with real-world nonstationary and nonlinear time series data, it is widely used in engineering, economics, earth and environmental sciences (e.g., Huang et al., 1998; Chang et al., 2003; Yu et al., 2008; Colominas et al., 2014; Derot et al., 2016). We use the most up-to-date noise-assisted improved CEEMDAN technique with at least hundreds of noise realizations to decompose observed and simulated PM_{2.5} time series. Readers can refer to Colominas et al. (2014) for a detailed description of the technique and access to the corresponding MATLAB code. Trial and error attempts are made in setting the input (standard deviation of the added noise and the limit of maximum number of sifting allowed) of the improved CEEMDAN function to achieve best mode separation. In a desired best

160 [mode separation, neighboring IMFs should have very limited levels of mode mixing, which can be fast screened based](#)
161 [on the time series of the decomposed IMFs and their power spectrum.](#)

162 The impact of boundaries on the decomposed annual cycles and the residual is assessed by the variations (standard
163 deviation) of hypothetical decomposed boundaries by cutting a continuous eighteen-year total PM_{2.5} observation
164 (North Little Rock, AR) 48 times at different years and times of the year (Fig. S1). The standard deviation is found to
165 largely diminish within half the annual cycles and could be negligible within one year for the annual cycle. This could
166 very possibly expand to IMFs with other characteristic scales. Yet, trend components (residuals) show variability
167 depending on the available time period after cutting. Most of the time, they follow the reference long-term trend
168 reflected either by the residual or the summation of the residual and the IMF with the longest temporal scale
169 decomposed from the eighteen-year PM_{2.5} (Fig. S1c). This is in line with our expectations as a trend should exist
170 within a given time span, following the definition in Wu et al. (2007): “The trend is an intrinsically fitted monotonic
171 function or a function in which there can be at most one extremum within a given data span”. Although very strict
172 data completeness requirement is employed for this study, it should not be conceived as a limitation of the method
173 itself. A sensitivity test based on a period of nine years of total PM_{2.5} observations at the same site with 99% data
174 coverage shows that even though variability of annual cycles and long-term trends increases with decreased data
175 availability (100%, 90%, ..., 10%), the structure of those components is consistent. The average of 40 realizations of
176 annual cycles and long-term trend components in each data-completeness scenario is in perfect alignment with that of
177 100% data completeness (Fig. S2 and S3). Given the fact that those 40 realizations in each scenario are based on
178 independent random samplings of the original observations, the increased variability could very possibly result from
179 the difference in the sampled data itself rather than the method. Thus, the robustness of improved CEEMDAN
180 decomposed annual cycles and long-term trend is justified. In fact, EMD has been proven to be an effective tool for
181 data gap-filling (Moghtaderi et al., 2012).

182

183



184

185 **Fig. 2. Decomposition of observed (blue) and simulated (red) 24-hour average total PM_{2.5} into 7 IMFs and a**
 186 **residual component (trend) at Quabbin Summit, MA using the improved CEEMDAN: (a) Time series of total**
 187 **PM_{2.5}, IMFs and the residual component (all with the unit of μg/m³); (b) Power spectrum of the corresponding**
 188 **time series. The colored numbers on the right side of time series are the mean period t_m in days, while the ones**
 189 **on the right side of the power spectrum are the peak period t_p in days, which are also indicated by the dashed**
 190 **vertical lines on the power spectrum. Note that the scales for the time series are not all the same. Also, all power**
 191 **spectra are in the log scale, and those of the IMFs are zoomed in with a range of 10⁰ to 10⁴ on the y-scale for**
 192 **better visual clarity (compared with 10⁻² to 10⁷ for total PM_{2.5} and the residual component).**

193

194 The characteristic period of each IMF can be estimated by the peak period t_p (days) where the power spectrum of the
 195 IMF peaks:

196
$$t_p = \frac{1}{f_p} \quad (2)$$

197 in which f_p is the frequency that the power spectrum peaks in the unit of number of cycles per day. The peak estimates
 198 can be biased if more than one high-power frequency is located closely close to each other within one IMF. Thus, the
 199 power spectrum and t_p is only used as a fast screening tool to determine if a desired decomposition is accomplished.

200 As an alternative approach, the mean period t_m can be estimated by:

201
$$t_m = \frac{\text{Time span}}{(n_{max}+n_{min}+n_{zero})/4} \quad (3)$$

202 where n_{max} , n_{min} and n_{zero} are the number of maxima, minima and zero-crossings, respectively, during the
 203 *Time span* (days). As the frequency decreases, the mean period estimates become less accurate because of the limited
 204 time span compared with the length of the cycle and should be carefully interpreted.

205 An example of the total PM_{2.5} decomposition with improved CEEMDAN at the QURE site shows modes ranging from
 206 very high frequency to very low frequency (IMF1 to IMF7) and a residual (Fig. 2). [No visible mode mixing can be](#)
 207 [detected in both the time series \(Fig. 2a\) and the power spectrum \(Fig. 2b\) of all IMFs.](#) Mean (t_m) and peak (t_p)
 208 estimations of the characteristic periods of each IMF are presented on the right side of each mode. Annual cycles and
 209 long-term trend components are well represented by IMF6 and the residual, with the remaining IMFs carrying weekly,
 210 sub-seasonal, seasonal, and inter-annual variations, respectively, for both observed and simulated PM_{2.5} (Fig. 2). We
 211 have noticed that in some rare cases, a spurious mode in the last IMF with synchronous signal and very close scales
 212 to its previous IMF exists. This is possibly due to the fact that the characteristic periods of those IMFs are in proximity
 213 to the span of the studied time span. In these cases, the last two modes are merged by adding ~~those two modes~~them
 214 together to conduct a detailed evaluation as discussed in Section 4.1.

215 3.2 Statistical metrics

216 EMD-decomposed IMFs and trend components allow for a detailed time-dependent evaluation of PM_{2.5} and provide
 217 a novel opportunity to trace the performances of specific scales back to the corresponding speciated components. Note
 218 that the trend component is the decomposed residual component from the PM_{2.5} in the unit of $\mu\text{g}/\text{m}^3$, and it is not the
 219 traditional concept of trend in concentration per time. In addition to a direct evaluation of its magnitude, we also
 220 calculated its derivative to identify the periods with higher or lower rate of change (concentration per time). Time-
 221 dependent intrinsic correlation (TDIC) is utilized to study the evolvement of the model performance for cyclic
 222 variations throughout time (Chen et al., 2010; Huang and Schmitt, 2014; Derot et al., 2016). It is a set of correlations
 223 calculated for IMFs over a local period of time I centered around time t :

224
$$I(t) = [t - \frac{t_w}{2}, t + \frac{t_w}{2}] \quad (4)$$

225 in which t is the center time for the calculation of the correlation and t_w is the moving window length. The minimum
 226 of t_w is set to be the local instantaneous period of the IMF (larger of that in observation or simulation) using the
 227 general zero-crossing method to ensure that at least one instantaneous period is included in calculating the local
 228 correlation coefficient (Chen et al., 2010). The maximum of t_w is the entire data period with a traditional overall
 229 correlation being calculated. The empty spaces in the pyramids used to depict the TDIC are an indication that the
 230 correlation is not statistically significantly different from zero. With both decomposed observed and modeled
 231 concentrations in a narrow scale range, the correlation would no longer be contaminated by coexisting signals of
 232 different scales (Chen et al., 2010).

233 In order to summarize the performance of the decomposed trend component and IMFs, the ratio of the mean
234 magnitudes of the trend components is defined as:

$$235 \quad r_{trend} = \frac{Mean_{CMAQ}}{Mean_{observation}} \quad (5)$$

236 where $Mean_{CMAQ}$ and $Mean_{observation}$ represent the mean of simulated and observed residual components
237 respectively. The ratio of the mean amplitude of each IMF is defined by Equation 6, where an example for the annual
238 cycles is provided:

$$239 \quad r_{annual} = \frac{RMS_{CMAQ,annual}}{RMS_{observation,annual}} \quad (6)$$

240 where $RMS_{observation,annual}$ and $RMS_{CMAQ,annual}$ represent the root mean square of observed and simulated annual
241 cycles respectively. Finally, the phase shift of an IMF n is defined ~~to be the~~ days an IMF decomposed from modeled
242 time series has to ~~be shifted in order to~~ maximize the achieve the highest correlation (R_{max}) with the corresponding
243 IMF ~~with similar scale~~ from observed $PM_{2.5}$ time series. In practice, n could be as much as a few cycles of the mean
244 period, t_m . Here, we limit the absolute number of shift days to not exceed a half cycle as a reference for the phase
245 shift of an IMF. Thus, n satisfies $-(t_m/2) \leq n \leq (t_m/2)$ with t_m being the larger mean period in observation or
246 simulation. It becomes $-0.5 \leq n/t_m \leq 0.5$ in terms of number of cycles.

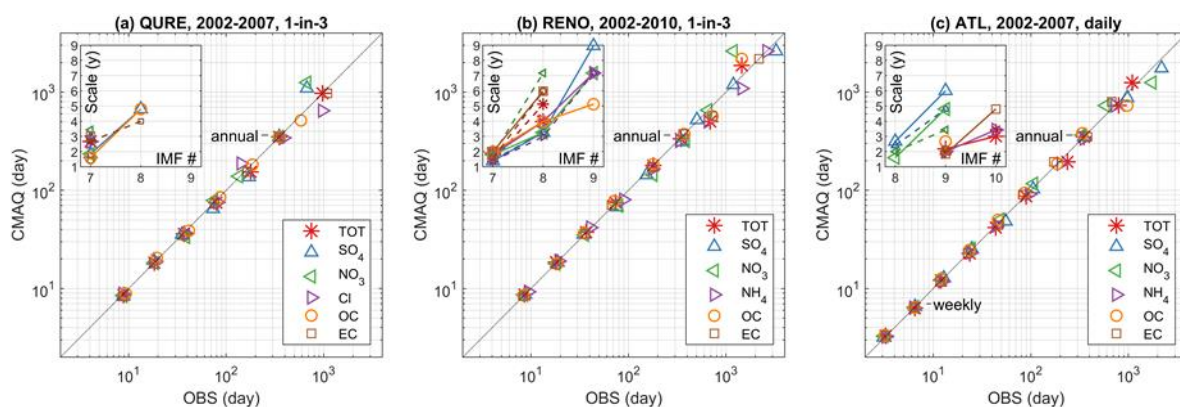
247 **4 Results and Discussion**

248 **4.1 Temporal scales**

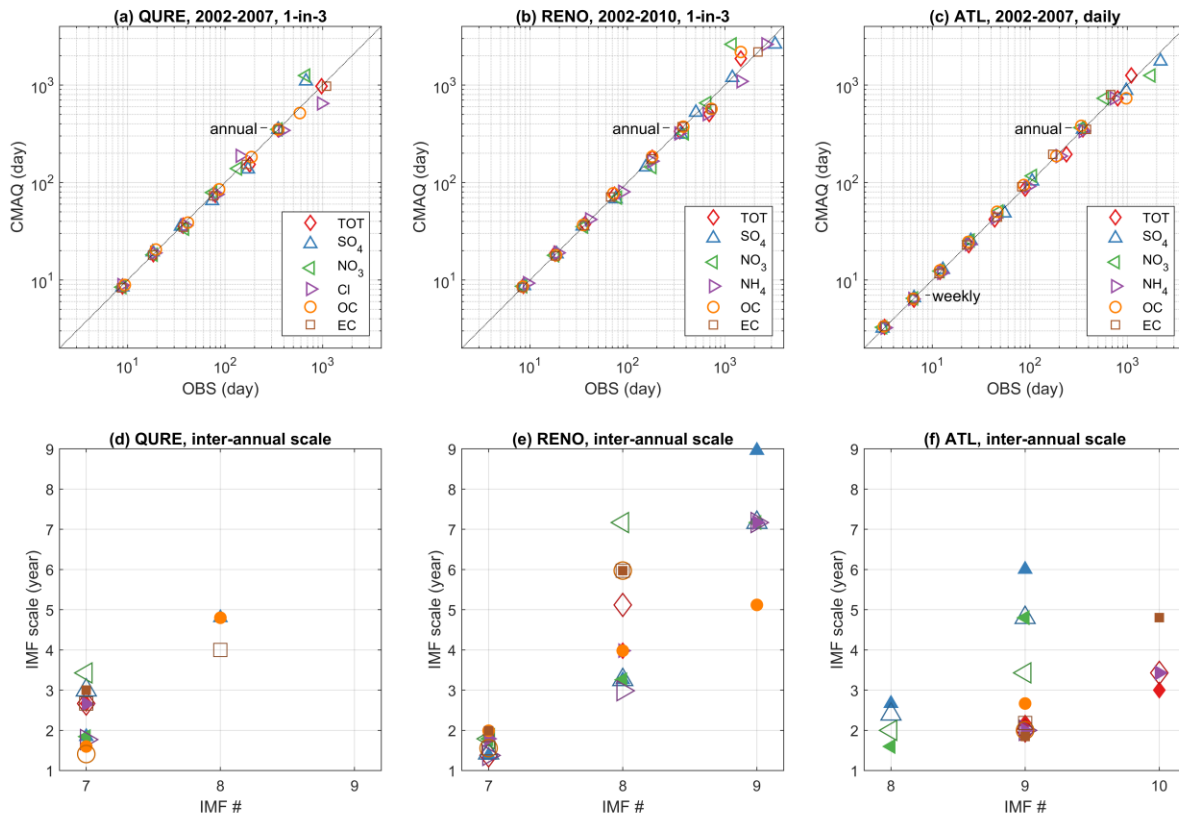
249 Temporal scales in $PM_{2.5}$ resolved by EMD depend solely on the intrinsic properties of the data itself. These properties
250 include underlying characteristics of specific $PM_{2.5}$ concentrations, the data sampling frequency, which determines the
251 scales that can be resolved in the high frequency IMFs, and the time span for the data coverage, which could possibly
252 play an important role in differentiating the low frequency IMFs from the trend component. Here, we first evaluate
253 the scales represented by the mean period in the speciated and total $PM_{2.5}$ time series. Since each IMF represents a
254 nonstationary process, the mean period t_m is only an estimate of its characteristic scales. Evaluation of t_m might not
255 necessarily be able to identify issues with corresponding model simulations~~Note that the mean period is only one~~
256 indication of the model evaluation against observations, and it does not indicate any information on the magnitude or
257 the phase of the time series, which is more important and will be further discussed in Sections 4.3 to 4.4.

258 Fig. 3a presents the characteristic scales (t_m) of IMFs in observed and simulated total and speciated $PM_{2.5}$ of QURE.
259 The CMAQ model compares well with the observations for IMFs 1 through 6 with cycles of 9, 19, 37, 78, 158 and
260 347 days (average of all observed and simulated total and speciated $PM_{2.5}$). Among all these IMFs, IMF6, which
261 represents the annual cycles, shows the least variations in the characteristic scale (Fig. 3a) and highest peak energy
262 from the power spectrum such as Fig. 2b for total $PM_{2.5}$, except for observed EC and OC where the power of half-
263 year cycles is more dominant (Fig. S4). These two features demonstrate a clear seasonality in both observed and
264 simulated total and speciated $PM_{2.5}$, which would otherwise be concealed by practices such as monthly averaging.

265 This can be further confirmed by the statistically significant annual cycles (except for observed EC and OC) (Fig. S5)
 266 based on a Monte Carlo verified relationship between the energy density and mean period of IMFs (Wu and Huang,
 267 2004; Wu et al., 2007). To explore the inter-annual cycles in more detail, mean periods of IMFs with scales longer
 268 than a year are being displayed in the top left panel of Fig. 3a. Some variability exists between the observation and
 269 model simulation to the extent that not all IMFs from observation are being simulated and vice versa [for the inter-](#)
 270 [annual cycles. The characteristic scales of all decomposed IMFs with scales longer than a year are shown in Fig. 3d.](#)
 271 The estimated mean periods of the inter-annual cycles and the differences in the presence of slow varying cycles with
 272 the long characteristic scales are likely to be influenced by their proximity to the data time span of 6 years (4 years for
 273 CI). This implies that the model evaluation shouldn't go beyond 3 years (2 years for CI) given the current data
 274 coverage. CMAQ captured the 3-year cycles in EC and total PM_{2.5} and 2-year cycles in OC and CI, despite an
 275 overestimation in the scales of 2-year cycles in observed SO₄ and NO₃.

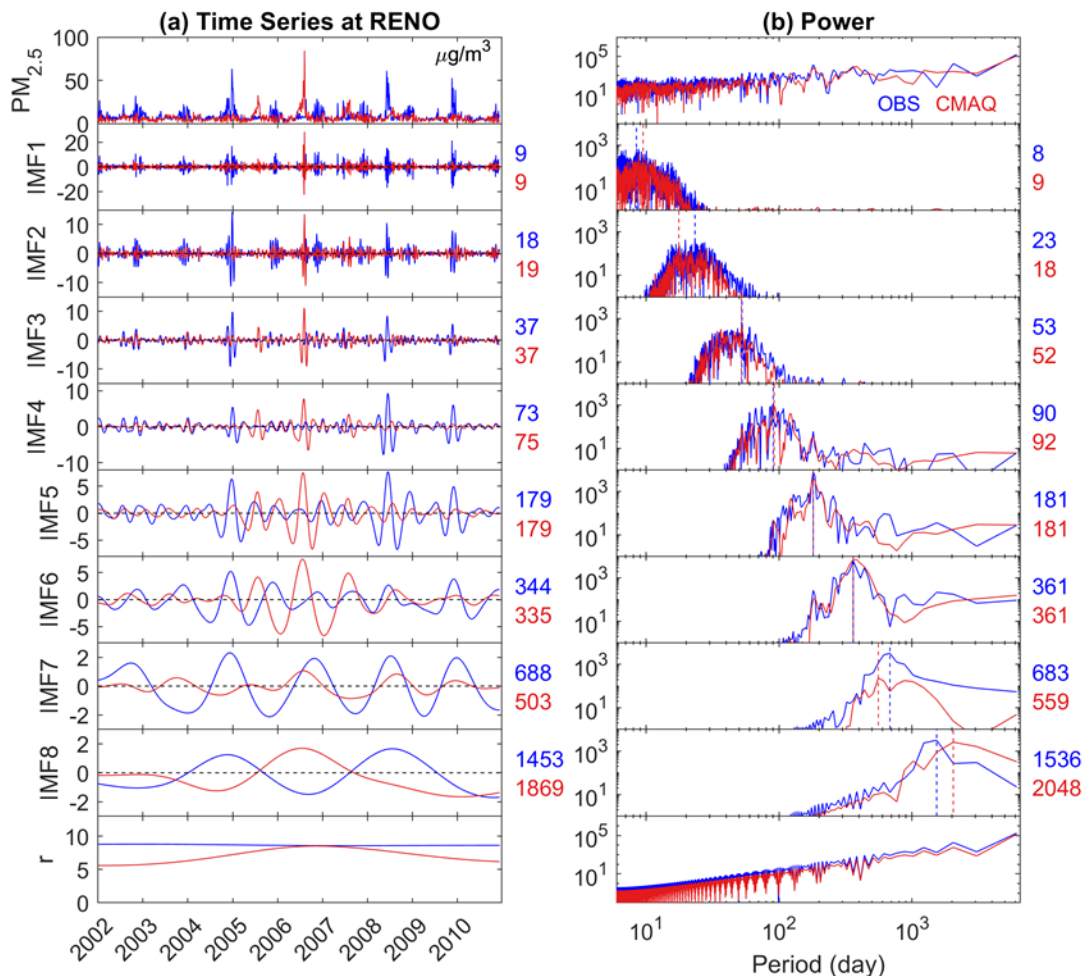


276



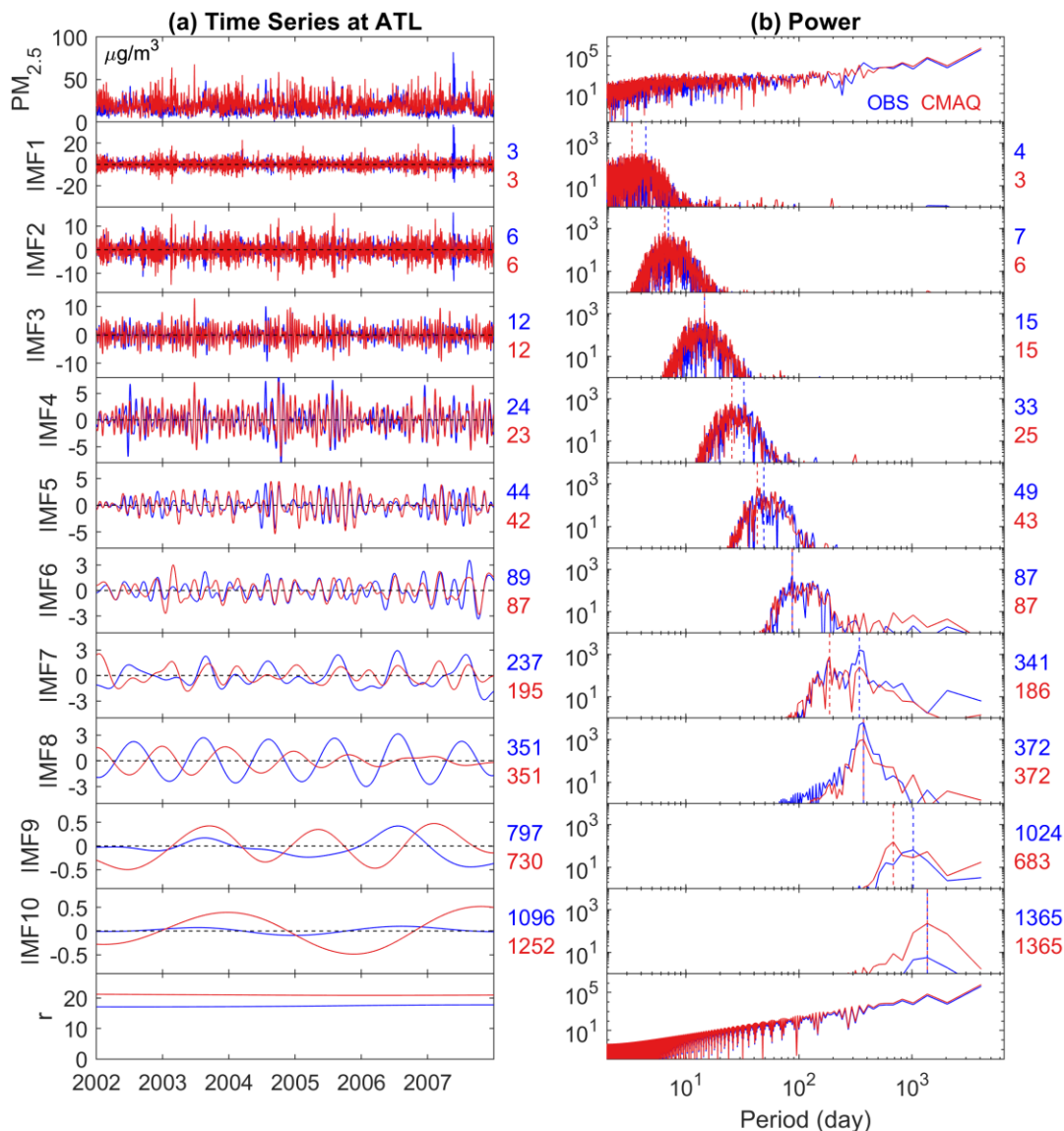
277
 278 **Fig. 3. The characteristic scales (t_m) resolved in the IMFs of observed and simulated total and speciated PM_{2.5}**
 279 **for (a, d) QURE, (b, e) RENO and (c, f) ATL. In (a-c), IMF1 to the last pair of IMFs with increasing**
 280 **characteristic periods are shown from bottom left to top right. Mean periods of IMFs with scales longer than a**
 281 **year are being displayed in (d-f) with the same shapes as in the legend above to show the characteristic scales**
 282 **of all decomposed IMFs given that not all IMFs from observation are being simulated and vice versa. Top-left**
 283 **panel in each subplot shows characteristic scales in the unit of years (y-axis) of all IMFs with inter-annual cycles**
 284 **(the x-axis represents the IMF number). In the (d-f) subplots, species decomposed from observations are shown**
 285 **with smaller filled shapes connected by solid lines, while species decomposed from simulations are represented**
 286 **by smaller markers/larger open shapes in slightly darker shades connected by dashed lines.**

287 Similar features in observed and simulated total and speciated PM_{2.5} concentrations at RENO are presented in Fig. 3b.
 288 Likewise, the highest peaks in the power spectrum also sit in the annual cycles of IMF6 except for the observed OC
 289 and total PM_{2.5} which have higher peak power at half-year cycles. All annual IMFs are statistically significant except
 290 for simulated NH₄ (Fig. S5). The small variation in the estimated characteristic period of IMF6 is because this
 291 monitoring site is located in a wildfire prone region on the border of Nevada and California. Clear evidence can be
 292 seen from Fig. 4a that an extra annual cycle in the IMF6 of observations in the summer of 2008 is depicted, which is
 293 very possibly driven by the 2008 California Wildfires spanning from May until November. [Satellite image of the](#)
 294 [wildfire smoke on July 10, 2008 can be found in Figure 1 from Gyawali et al. \(2009\).](#) Unlike the diversified scales in
 295 IMF7 at QURE, IMF7 at RENO features universal 2-year cycles of all species as well as total PM_{2.5} and all of them
 296 are well replicated by the model. However, variations in time scales are present in IMF8 possibly because of the
 297 limited data coverage. Thus, only species with time scales less than 4 years in both observations and model simulations
 298 are evaluated. It is evident that CMAQ has reproduced the 3-year cycles in SO₄ and NH₄.



299
 300 **Fig. 4.** Same as Fig. 2 but for the RENO site with 8 IMFs.
 301

302 ATL is the only speciated site with daily data coverage. Observed and simulated total and speciated $PM_{2.5}$
 303 concentrations at the ATL site are decomposed into 9 or 10 IMFs (Fig. 3c). Because of the change in data frequency,
 304 high frequency scales such as weekly cycles can be evaluated and the significance tested (Fig. S5) annual cycles with
 305 the highest peak power is represented by IMF8 (IMF7 for SO_4 and NO_3). Annual cycles of SO_4 and NO_3 appeared in
 306 the earlier stage of decomposition in IMF7 because of their relatively weak half-year cycles, which largely led to the
 307 mixed signal of half-year and annual cycles in IMF7 in total $PM_{2.5}$ as in Fig. 5b. This is more visible in the
 308 observed IMF7 where the energy of the one-year period surpasses that of the half-year. Yet, clues can be seen from
 309 Fig. 5 that the amplitude and the energy of annual cycles leaked into IMF7 is very limited compared to that remaining
 310 in IMF8, indicating that it is still safe to conduct model evaluation on the seasonality using IMF8 with an
 311 underestimation in the amplitude of observation. On the other hand, inferences should be made with caution for IMF7
 312 because of the mixed modes. Scales up to 3 years are relatively well reproduced by the model.



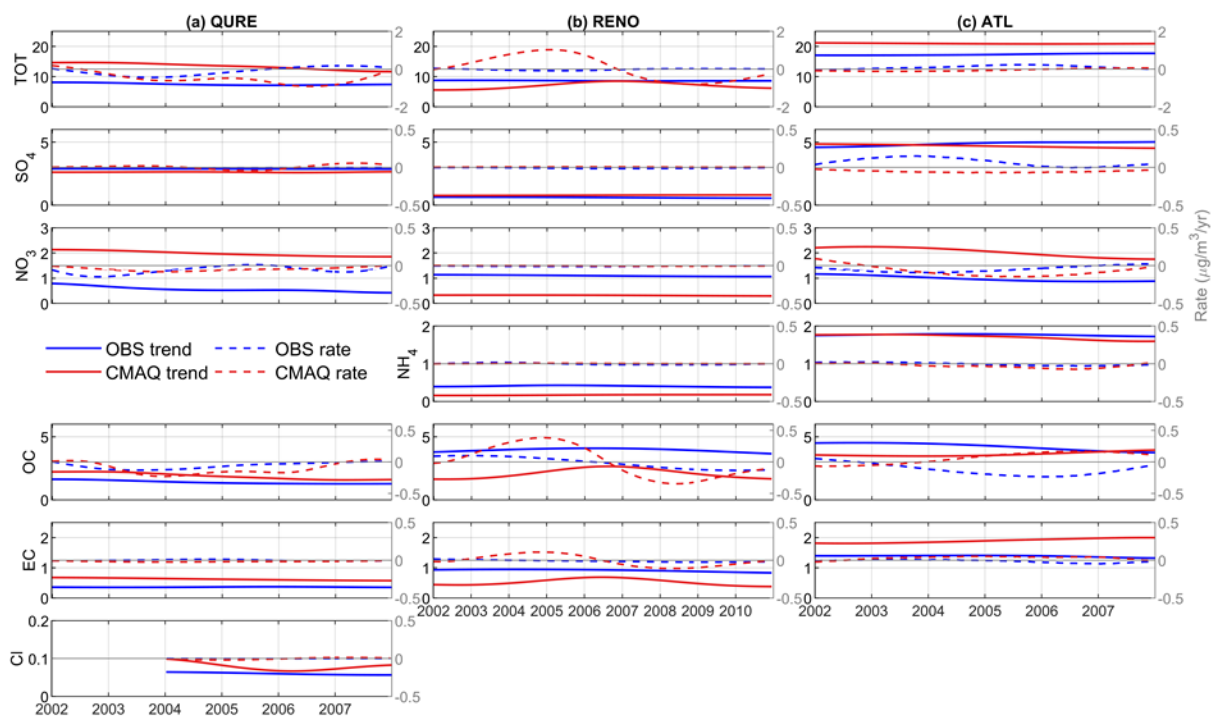
313

314 Fig. 5. Same as Fig. 2 but for the ATL site with 10 IMFs.

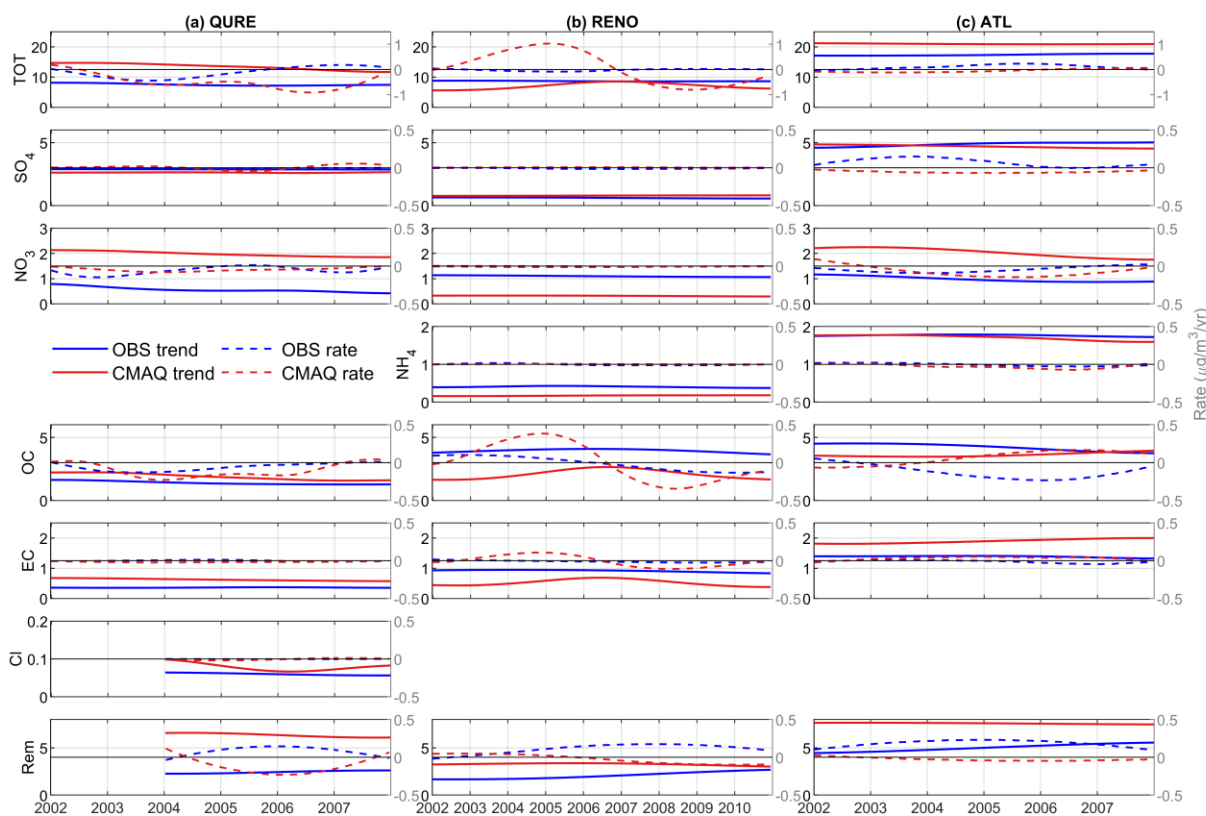
315 4.2 Long-term trend

316 The EMD-decomposed long-term trend components for the observed and simulated total and speciated $PM_{2.5}$
 317 concentrations are presented in Fig. 6. To better visualize the non-linearity of the trend component, the rates of change
 318 (temporal derivative of a trend component, which is the change in the consecutive concentration divided by the
 319 sampling rate of 1 or 3 days and converted to the unit of $\mu g/m^3/year$ by multiplying 365 day/year) are added with a
 320 separate y-axis on the right side in each panel (gray colored scale). It is evident that $PM_{2.5}$ is changing at a varying
 321 rate, forming either a monotonic trend component or a trend component with one extremum, which cannot be fully
 322 represented by a single constant number using a traditional linear regression approach. Given that there are chemical

323 species ([the remaining component, *Rem*](#)) other than the ones studied in the total $PM_{2.5}$, not all performance issues can
324 be fully explained by the five available species.



325



326
 327 **Fig. 6. Trend components of observed and simulated total and speciated PM_{2.5} for (a) QURE, (b) RENO and (c)**
 328 **ATL in $\mu\text{g}/\text{m}^3$, with dashed lines representing the rate of the change (temporal derivative of the trend**
 329 **component converted to $\mu\text{g}/\text{m}^3/\text{year}$) are plotted against the right-side y axis, with a reference line of no change**
 330 **in dark gray/black line in the center. Note that the scales are not all the same.**

331
 332 At the QURE site, CMAQ captures the general decreasing trend in observed total PM_{2.5} which can mainly be traced
 333 back to NO₃ and OC and the remaining components, while both observed and simulated trend components in SO₄
 334 and EC are relatively constant (Fig. 6a). The relative importance of each component in driving the trend of observed
 335 and simulated total PM_{2.5} reflected by its mean concentration share is summarized in Table 1 (time-dependent
 336 variations of the concentration share is attached in Fig. S6 for reference). Moreover, the periods with highest
 337 decreasing rate in observed total PM_{2.5} during 2003-2004 with a decreasing rate of $-0.44 \mu\text{g}/\text{m}^3/\text{year}$ is also well
 338 replicated by the model. Nevertheless, the slightly increasing PM_{2.5} level in the later years is simulated to be decreasing
 339 at a much higher rate, which is partly due to the overestimated decreasing rate in OC and species other than the five
 340 studied ones. The trend component of simulated Cl shows a cyclic-like feature because of proximity between the
 341 existence of a cycle of 4-5 years (by decomposing the simulation during the 6-year study period) and 4-year period
 342 limited by the available quality assured observations. The rate of change in the simulated trend component by

343 decomposing the simulation during the 6-year study period would mimic that from the 4-year observation, both with
 344 a negligible negative value throughout 2004-2007. However, the mean magnitude of the trend component is almost
 345 doubled twice as high (1.8 times compared with observation) in the model with contribution from all species except
 346 for SO₄. A quantitative summary of the comparison between the mean magnitudes of the observed and model trend
 347 components can be found in Table 42.

348 **Table 1.** Concentration share (%) of different components in total PM_{2.5}. It is estimated by dividing the mean trend
 349 components of each species by that of total PM_{2.5} for both OBS and CMAQ, multiplied by 100. The concentration
 350 share of *Rem* is estimated by subtracting all the available species share from 100 to compensate for the small
 351 discrepancies caused by the rounding up process and uncertainty in the mode decomposition. “-” indicates the data is
 352 not available (same applies for all other tables).

		<u>SO₄</u>	<u>NO₃</u>	<u>NH₄</u>	<u>OC</u>	<u>EC</u>	<u>Cl</u>	<u>Rem</u>
<u>QURE</u>	<u>OBS</u>	<u>38</u>	<u>7</u>	<u>-</u>	<u>19</u>	<u>5</u>	<u>1</u>	<u>30</u>
	<u>CMAQ</u>	<u>19</u>	<u>15</u>	<u>-</u>	<u>14</u>	<u>5</u>	<u>1</u>	<u>47</u>
<u>RENO</u>	<u>OBS</u>	<u>7</u>	<u>13</u>	<u>5</u>	<u>46</u>	<u>11</u>	<u>-</u>	<u>20</u>
	<u>CMAQ</u>	<u>11</u>	<u>4</u>	<u>2</u>	<u>30</u>	<u>7</u>	<u>-</u>	<u>45</u>
<u>ATL</u>	<u>OBS</u>	<u>28</u>	<u>6</u>	<u>10</u>	<u>24</u>	<u>8</u>	<u>-</u>	<u>24</u>
	<u>CMAQ</u>	<u>22</u>	<u>10</u>	<u>8</u>	<u>17</u>	<u>9</u>	<u>-</u>	<u>33</u>

353
 354 **Table 42.** The ratio of mean magnitude of the trend component r_{trend} (CMAQ/observation). Boldface values indicate
 355 a relatively good estimate of the magnitude (0.7 - 1.3). “-” indicates the data is not available (same applies for Tables
 356 2 and 3).

	TOT	SO ₄	NO ₃	NH ₄	OC	EC	Cl
QURE	1.8	0.9	3.5	-	1.4	1.7	1.3
RENO	0.8	1.3	0.3	0.4	0.5	0.6	-
ATL	1.2	1.0	2.1	1.0	0.9	1.4	-

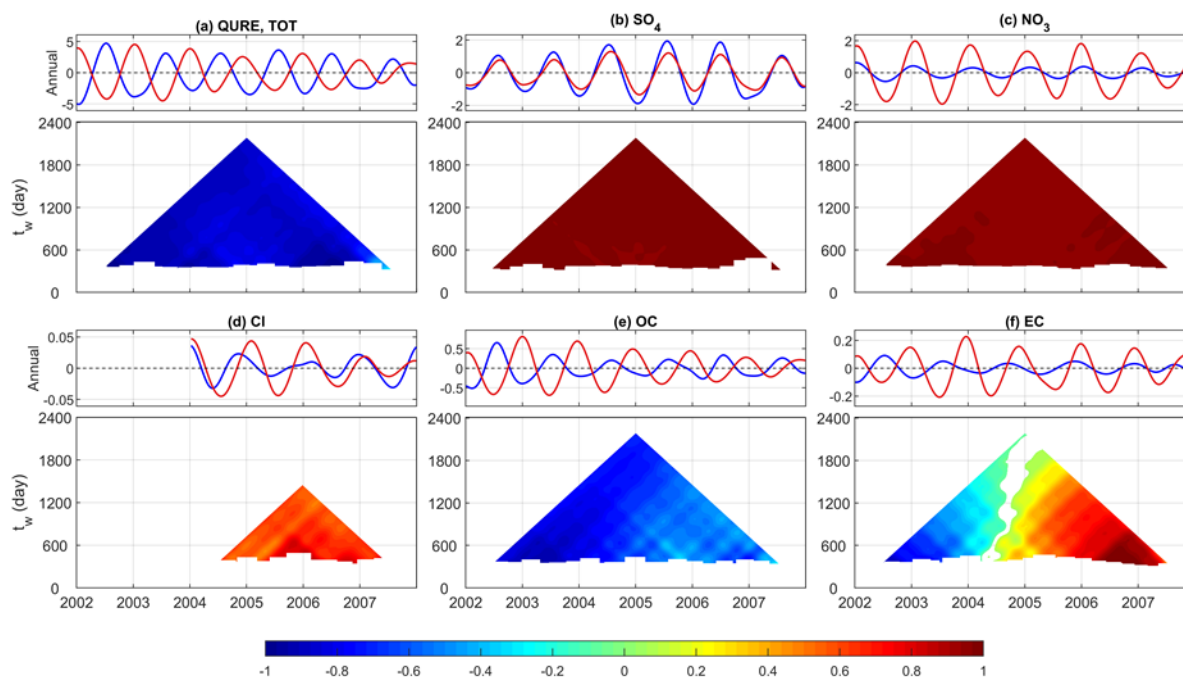
357
 358
 359 RENO is located close to the border with California and is affected by large wildfire breakouts in the western U.S.
 360 (Gyawali et al., 2009) as can be seen in the spikes of the observed total PM_{2.5} (Fig. 4a). Thus, OC makes up a much
 361 larger portion of total PM_{2.5} compared to other locations (Table 1). The model simulates large increasing rate up to
 362 1.03 µg/m³/year and decreasing rate up to -0.80 µg/m³/year before and after the 2006-2007 winter season and fails to
 363 reproduce the relatively stable condition seen in the observations with only -0.09 µg/m³/year decreasing in 2004-2005
 364 and 0.04 µg/m³/year- increasing in 2008-2009 (Fig. 6b). Similar feature is found for combustion-related OC and EC
 365 species. The observed slightly decreasing trends in SO₄ and NH₄ during 2005-2009 are not being captured in the model
 366 simulations. The magnitude of the trend component is slightly underestimated with r_{trend} of 0.8 with contribution
 367 from all species except for SO₄ as well (Table 42).

368 During the period of 2002-2007, observations at ATL reveal a slightly increasing $PM_{2.5}$ trend that cannot be explained
369 by the five ~~listed-available~~ $PM_{2.5}$ components trend (Fig. 6c), ~~possibly~~ indicating a contribution of the remaining
370 species such as the non-carbonaceous portion of organic matter. Non-carbonaceous organic matter can account for
371 more than half of total organic matter, which, in turn, can account for a large portion of the total $PM_{2.5}$ mass (Edgerton
372 et al., 2005). In contrast, the model shows a slight decreasing trend with a peak decreasing rate in 2003 and misses the
373 peak increasing rate of $0.23 \mu\text{g}/\text{m}^3/\text{year}$ in the winter season of 2005. Similarly, reversed trends are also simulated for
374 SO_4 , OC and EC, while the change rate in NO_3 is well captured. Unlike the previous sites, magnitude of trend
375 components in total and speciated $PM_{2.5}$ are well simulated except for EC (1.4 times the observation) and NO_3 (2.1
376 times).

377 To sum up, the [decreasing](#) long-term trend at QURE is well simulated by the model. The occurrence of large wildfires
378 lasting for several months [have-has](#) significantly impacted the long-term trend component at RENO and the model
379 failed to capture those combustion-related species and total $PM_{2.5}$ primarily due to limitations in the historical data
380 used to specify day-specific wildfire emissions (Xing et al., 2013). Slightly increasing levels of $PM_{2.5}$ and its species
381 observed at ATL are simulated to be slightly decreasing, except for NO_3 which is well simulated. The magnitude of the
382 long-term trend components of total $PM_{2.5}$ and SO_4 are well represented by CMAQ (Table [42](#)). The model performs
383 differently across the sites in terms of the magnitudes of the trend component in NO_3 , NH_4 , Cl, OC and EC. [The large](#)
384 [discrepancy in the magnitude of some long-term trend components is likely pointing to the systematic bias in the](#)
385 [annual emission estimations as discussed in Xing et al., \(2013\), which mainly focused on long-term trend rather than](#)
386 [the absolute level of the emissions.](#) Species other than those in the available dataset ~~may~~ also play a considerable role
387 in driving the agreements or disagreements between model simulations and observations of total $PM_{2.5}$.

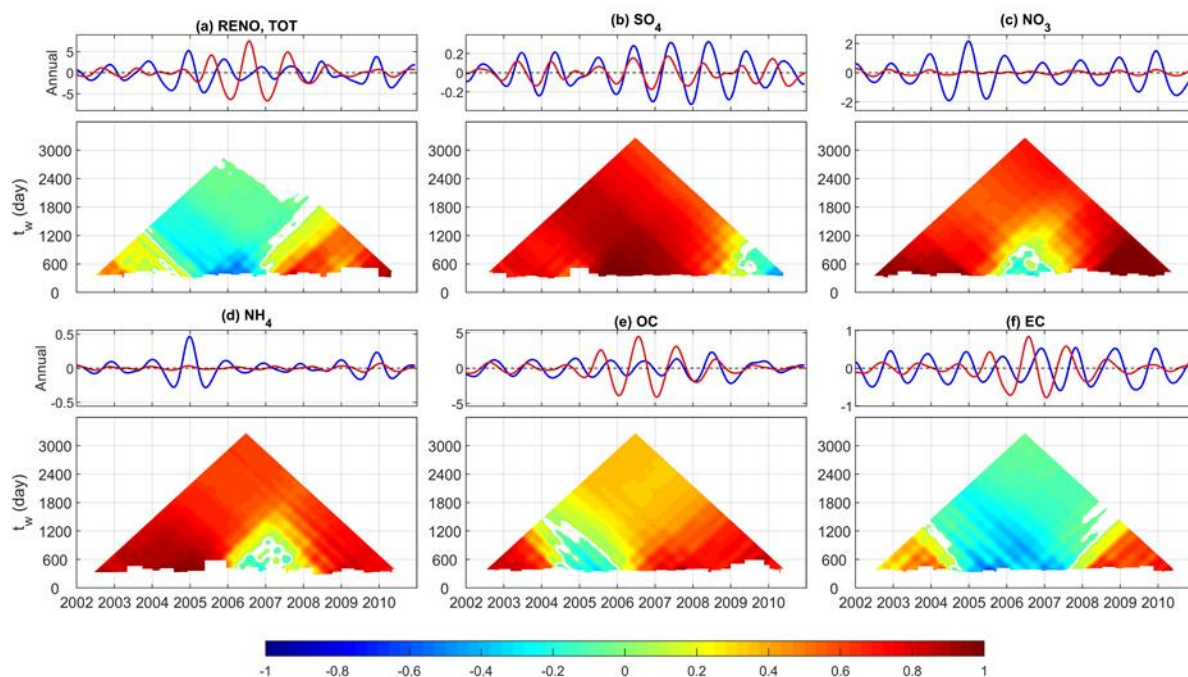
388 4.3 Seasonality

389 The EMD-assisted seasonality evaluations utilize the decomposed IMFs with characteristic period of one year to
390 evaluate the amplitude and phase of the model simulation, both of which are time-dependent. [As mentioned in Section](#)
391 [4.1, these IMFs are statistically significant from white noise with few exceptions \(Fig. S5\).](#) We first demonstrate the
392 evaluation for total $PM_{2.5}$ at QURE (Fig. 7a). The top panel shows the annual cycle components and the bottom panel
393 shows its TDIC pyramid. The decreasing amplitude of the annual cycles throughout 2002-2007 is almost perfectly
394 represented with an overall ratio r_{annual} being 1.0 (Table [23](#)). Each pixel in the TDIC pyramid is the correlation
395 (color-coded) calculated during a period of time $I(t)$ with width of t_w days (y-axis) centered at a specific day (x-axis)
396 as introduced in Section 3.2. The annual cycle mean periods are identical between CMAQ and observations (350 days,
397 Fig. 2a IMF6), but there is a phase shift for all years with the entire TDIC pyramid being close to -1. By shifting the
398 CMAQ annual cycles backward 159 days (almost half year), the overall correlation of the annual component can reach
399 up to a peak of 0.9 (Table [34](#)).



400
 401 **Fig. 7. Decomposed annual cycles (IMF6) from observed (blue) and simulated (red) concentrations ($\mu\text{g}/\text{m}^3$) of**
 402 **(a) total $\text{PM}_{2.5}$, (b) SO_4 , (c) NO_3 , (d) Cl , (e) OC and (f) EC and their corresponding TDIC at Quabbin Summit,**
 403 **MA. The window size t_w indicates the width of the window used to calculate a specific correlation centered at**
 404 **the day represented in x-axis.**

405 What are the driving factors for the above phase shift in modeled total $\text{PM}_{2.5}$ at Quabbin Summit, MA? The illustrations
 406 in Fig. 7a for total $\text{PM}_{2.5}$ alone cannot provide useful information that will allow the modeler to improve the model's
 407 performance. This is accomplished by applying the EMD method to the $\text{PM}_{2.5}$ speciated components (Fig. 7b-f). Traces
 408 of the semi-annual phase shift (-159 days) of annual cycles or large overestimation in the winter and underestimation
 409 in the summer is because of the largely overestimated amplitude of NO_3 (4.3 times that of observation) which peaks
 410 in the winter and the almost semi-annual shifted OC (-147 days), as well as contributions from EC and Cl . NO_3 has a
 411 mean amplitude reaching almost half of that of the total $\text{PM}_{2.5}$. OC directly drives both the observed and simulated
 412 annual components to be negatively correlated. EC follows the feature of OC in the first four years or so and the
 413 feature of NO_3 in 2006 and 2007 and contributes to the half year shifted total $\text{PM}_{2.5}$. The magnitude of winter-peaking
 414 Cl cycles are overestimated with a phase shift of one month. However, the contribution of Cl is very limited because
 415 of the tiny amplitude in both observed and simulated annual cycles. In addition, annual cycles in SO_4 are well
 416 reproduced for the entire time span with an amplitude ratio of 0.7. A quantitative summary of the evaluation of the
 417 annual cycles at this site can be found in Tables 2-3 and 34.



418

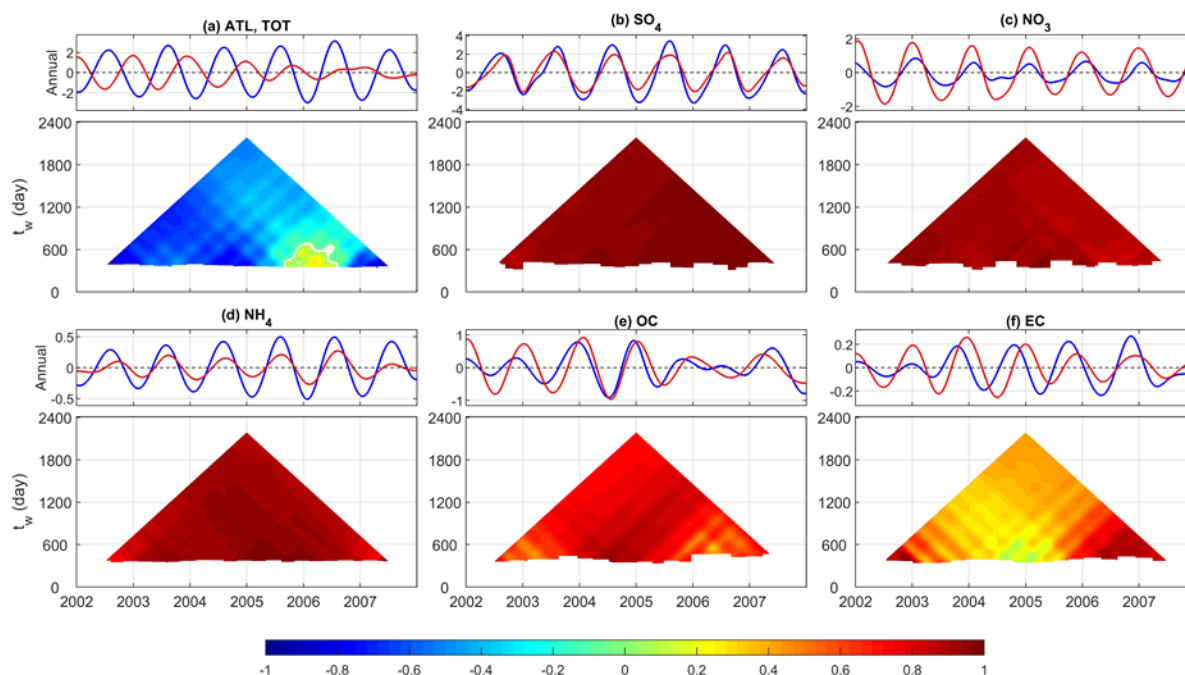
419 **Fig. 8. Same as in Fig. 7 for Reno, NV, except that (d) represents NH₄ rather than Cl.**

420 Both observed and simulated annual cycles at the RENO site are largely [contaminated-influenced](#) by the extreme
 421 events lasting for several months that are not properly simulated, indicating the need for more [accurately specified](#)
 422 [wildfire emissions-appropriate emissions allocation](#). Overall, annual variations for total and speciated PM_{2.5} are largely
 423 underestimated except for the total PM_{2.5} and combustion-driven EC and OC from 2005 to 2007 (Fig. 8). The modeled
 424 phase of SO₄, NO₃, NH₄ and OC agrees with that of observation with [the](#) exception for a length of about two years in
 425 each that missed the phasing: 2009-2010 for SO₄, summer 2005-summer 2007 for NO₃, 2006-2007 for NH₄ and 2004-
 426 2005 for OC. It is also notable that the TDIC pyramid of EC mimics that of total PM_{2.5}, implying the existence of
 427 errors in modeled EC in processes such as emissions, transport, and deposition that affected the model performance
 428 for total PM_{2.5}. In comparison, SO₄ and OC are relatively well simulated with a mean amplitude ratio of 0.5 and 1.5
 429 and a phase shift of 36 and 33 days, respectively.

430 Observed annual cycles of total PM_{2.5} at the ATL site features a slightly increasing amplitude of annual variations
 431 from 2002 to 2006 which then decreased to the original state in 2007 (Fig. 9a). Conversely, model-simulated annual
 432 cycles became weaker throughout the period, with an overall r_{annual} of 0.5. As at the QURE site, the simulated annual
 433 components at the ATL site also show a shift of several months (-132 days). Specifically, traces of these phase shifts
 434 or large overestimation in the winter and underestimation in the summer can be seen from the more than doubled
 435 amplitude of NO₃ which peaks in winter and underestimated SO₄ and NH₄ in the warm seasons as well as the -54 days
 436 shifted EC. The anti-correlated remaining species other than those in the available dataset clearly played a role in
 437 driving the discrepancies seen in the total PM_{2.5} annual cycles (Fig. 10). Specifically, the anti-correlation likely points
 438 to an inaccurate representation of the seasonal variation of the non-carbonaceous portion of organic matter due to an
 439 [incomplete-improper](#) representation of organic aerosols in the model version analyzed here; [newer versions of the](#)

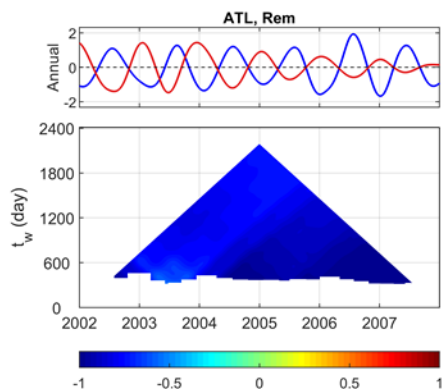
440 [CMAQ model include updated treatment of organic aerosols \(e.g., additional SOA formation pathways, improvements](#)
 441 [in representation of primary OM emissions\) which is likely to correct the mentioned features \(Appel et al., 2017;](#)
 442 [Murphy et al., 2017; Xu et al., 2018\)](#)~~this problem has since been corrected in more recent releases of the CMAQ~~
 443 [model](#). The underestimated annual variations in the remaining components closely resemble that of the annual
 444 variation in total PM_{2.5}. The phase of simulated SO₄, NO₃, NH₄, and OC species is in good agreement with those in
 445 observations and the amplitude of simulated annual cycles in SO₄, OC and EC agree well with that in the observations
 446 (Tables 2-3 and 3-4).

447 In sum, annual cycles of PM_{2.5} are also time-dependent and the phase in the annual cycles for total PM_{2.5}, OC and EC
 448 reveals a general shift of up to half a year (Table 3-4); this indicates a potential problem in the allocation of emissions
 449 during this study period and/or the treatment of organic aerosols in this version of the model. CMAQ generally
 450 simulated the phase in SO₄, NO₃, Cl and NH₄ quite well but did not always capture the magnitude of their variations
 451 (Table 2-3).



452
 453 **Fig. 9.** Same as in Fig. 7 for Atlanta, GA, except that the annual component is resolved in IMF8 (IMF7 for SO₄
 454 and NO₃) because of the difference in sampling rate and characteristic embedded in the time series at ATL and
 455 (d) represents NH₄ rather than Cl.

456



457
 458 **Fig. 10.** Decomposed annual cycles in Atlanta, GA for the remaining components presented in total PM_{2.5} other
 459 than the five species in Fig.9.

460 **Table 32.** The ratio of mean amplitude of the annual component r_{annual} (CMAQ/observation). Boldface values
 461 indicate a magnitude with a ratio close to 1 (0.7 -1.3).

	TOT	SO ₄	NO ₃	NH ₄	OC	EC	Cl
QURE	1.0	0.7	4.3	-	1.6	3.1	1.6
RENO	1.2	0.5	0.1	0.2	1.5	0.9	-
ATL	0.5	0.7	2.4	0.4	1.2	1.0	-

462
 463 **Table 43.** Phase shift (n) of CMAQ simulated annual cycle components in days. The background color indicates the
 464 maximum correlation (R_{max}) that can be reached by shifting the CMAQ time series n days with respect to
 465 observations: white = [0.8, 1], light grey = [0.6, 0.8), grey = [0.4, 0.6), dark grey = (0.2, 0.4). The bold shows number
 466 of shifts less than a month while the italic shows shifts longer than three months.

	TOT	SO ₄	NO ₃	NH ₄	OC	EC	Cl
QURE	-159	-6	3	-	-147	-105	-30
RENO	78	36	12	-21	33	96	-
ATL	-132	0	8	-17	-24	-54	-

467
 468 **4.4 Sub-seasonal and inter-annual variability**
 469 In this section, model performance at multiple sub-seasonal and inter-annual scales with cycles less than 3 years,
 470 presented in the total and speciated PM_{2.5}, is evaluated following an approach similar to that for the annual cycles in
 471 Section 4.3 (Fig. 11). First, IMFs from observations and model simulations are paired based on their characteristic
 472 periods following the discussion in Section 4.1. Then, the magnitude of specific scales is evaluated using r_{IMFn}
 473 following Equation 6 of the r_{annual} for annual cycles. The phase shifts of the time series are assessed by the proportion
 474 of shifted days relative to the mean characteristic scales of the corresponding observed and simulated IMFs (n/t_m).

475 For example, a phase shift of 0.1 cycles in the 2-year cycles is approximately 73 days while it would be 18 days for
476 the half-year cycles.

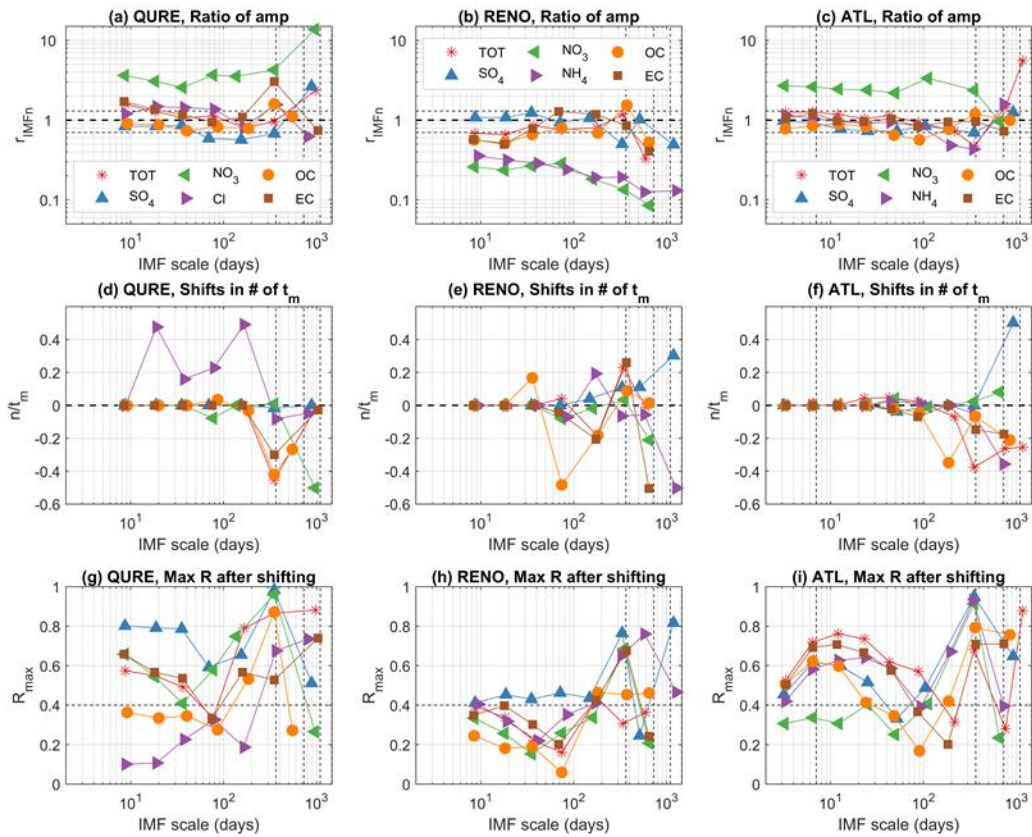
477 The performance of the simulated amplitude of the sub-seasonal and inter-annual cycles is relatively stable from a few
478 days to semi-annual scales and r_{IMFn} is close to 1 in most cases (Fig. 11a-c). CMAQ captures the features seen in the
479 observations at QURE, except for the large overestimation of NO_3 (r_{IMFn} ranges from 2.6 to 3.7 at the sub-seasonal
480 scale and reaches up to 13.8 for the 3-year cycles). Similar overestimation of NO_3 is also found at ATL (r_{IMFn} ranges
481 from 2.0 to 3.4, except for the 2-year cycles). In contrast, NO_3 at RENO is strongly underestimated with r_{IMFn} ranging
482 from 0.1 to 0.3 and reaching its minimum at the 2-year cycles. Likewise, all time scales of NH_4 at RENO are also
483 being underestimated with r_{IMFn} decreasing from 0.4 to only 0.1 at the 3-year cycles. The coexistence of
484 underestimation of NO_3 and NH_4 variability, as well as their trend component, likely points to the insufficient grid
485 resolution in representing ammonium nitrate episodes associated with stagnant meteorology in the mountainous
486 regions as illustrated by Kelly et al. (2019). To sum up, model has simulated the magnitude of features across all scales
487 in most of the studied cases. However, fluctuations in NO_3 are constantly being largely over- or under-estimated and
488 improvements to the model are required to better replicate its variability (Fig. 11a-c).

489 A high R_{max} of corresponding IMFs can only be achieved when the characteristic scales of those from observations
490 and model simulations are close, there is minimal mode mixing, and negligible irregular change of amplitude exists
491 during the study period. Thus, R_{max} tends to be small for all oscillations at RENO because of the irregular impact
492 from events such as wildfires. Thus, the interpretation of phase shift is focused on the components and time scales
493 having correlations above 0.4 only.

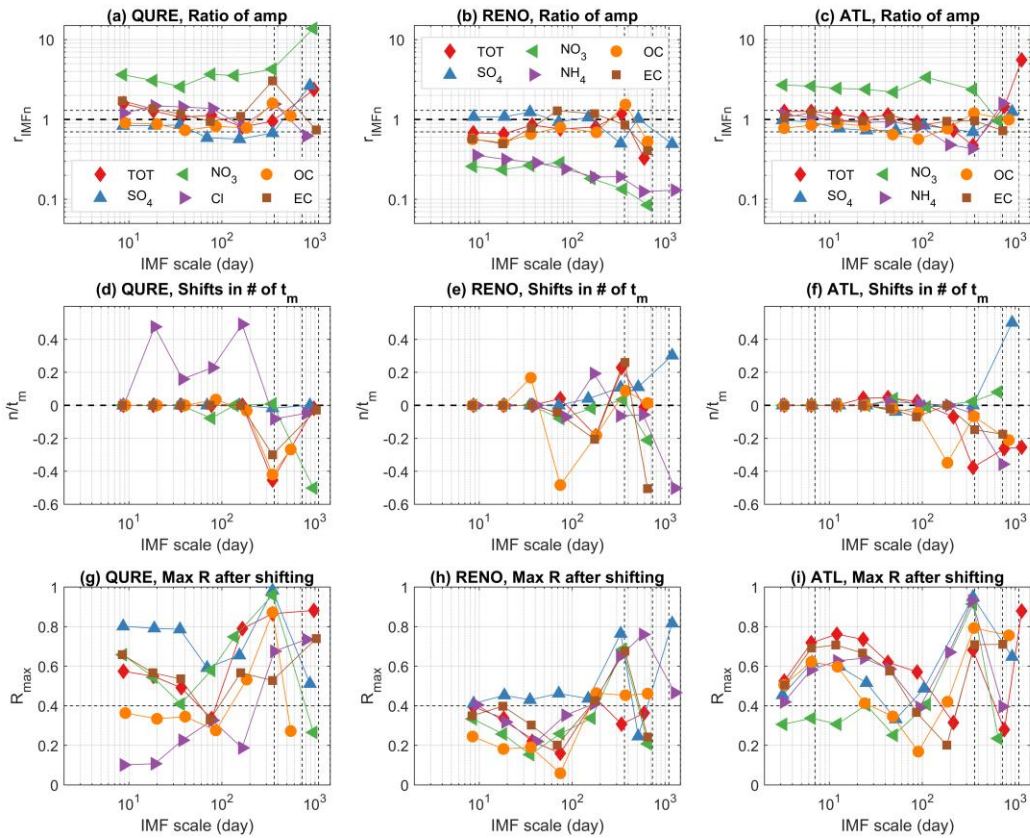
494 Results show that the sub-seasonal cycles at QURE all have a negligible phase shift of less than 0.1 cycles (Fig. 11d).
495 The semi-annual cycles at RENO have around 0.2 cycle phase shifts in total $\text{PM}_{2.5}$ (-0.2), NH_4 (0.2), OC (-0.2), and
496 EC (-0.2) while negligible phase shifts of less than 0.1 cycles are simulated in SO_4 ranging from 9 days to semi-annual
497 in scale. As at QURE, multiple sub-seasonal cycles at ATL all have a negligible phase shift of less than 0.1 cycles,
498 with the exception of semi-annual OC which has a phase shift of nearly -0.4 cycles with a marginal correlation of
499 around 0.4. Unlike the relatively stable R_{max} throughout the time scales within each of the species for QURE and
500 RENO, the R_{max} at ATL tends to be much higher (roughly 0.6-0.8) in the scales of 6 to 25 days, except for NO_3 ,
501 indicating the model's success in simulating those weather-induced air quality fluctuations at this site as reflected by
502 their negligible phase shifts.

503 However, the physical meaning of each sub-seasonal IMF is not yet fully understood and requires further study.
504 [Synoptic](#) For example, [synoptic](#) scale IMFs (IMFs with scale less than/around a month) usually have large variance
505 and are not statistically significantly different from white noise except for observed SO_4 and NH_4 (Fig. S5). Yet,
506 observed and simulated total and some speciated $\text{PM}_{2.5}$ at QURE and ATL (except IMF1) can achieve moderate to
507 high R_{max} at these time scales (Fig. 11 g-i), indicating a potential physical explanation of those time scales using
508 meteorological variables. IMFs with scales longer than a month but less than half year possess much less variance and
509 are usually not statistically significantly different from noise. Exceptions are also found at the Atlanta site where

510 observed IMFs are mostly significantly different from noise. Whereas semi-annual cycles are mostly statistically
 511 significant (note that semi-annual SO_4 and NO_3 at ATL are too weak to be decomposed into a separate IMF). In a
 512 previous study, He et al. (2014) found semi-annual oscillations in the corrected AERosol RObotic NETwork
 513 (AERONET) Aerosol Optical Depth (AOD) and PM_{10} mass concentrations are primarily caused by the change of
 514 wind directions in Hong Kong.



515



516

517 **Fig. 11. Model performance at all temporal scales for sites QURE, RENO and ATL. (a-c) ratio of mean**
 518 **amplitude of corresponding IMFs with similar characteristic mean periods (ideal ratio=1.0); (d-f) the phase**
 519 **shift n in the number of mean periods (average mean period of corresponding IMFs decomposed from**
 520 **observation and model simulation); (g-i) maximum correlation R_{max} can be achieved by shifting the modeled**
 521 **time series. The average mean period of corresponding IMFs decomposed from observations and CMAQ of**
 522 **total and speciated $PM_{2.5}$ are represented on the x-axis; all metrics on the y-axis are unitless. Horizontal**
 523 **reference lines are drawn at 0.7 and 1.3 in (a-c). Weekly, annual and inter-annual (2- to 3-year) scales are**
 524 **marked with vertical dashed lines.**

525 The evaluation and interpretation of inter-annual cycles are constrained by the limited available speciated observations
 526 for a period of 6 to 9 years (4 years for Cl at QURE). Thus, only 2- to 3-year cycles are presented (Fig. 11) and
 527 evaluated. Among the 2- to 3-year inter-annual cycles at QURE, there is minimal phase shift for total $PM_{2.5}$, SO_4 , Cl,
 528 and EC with moderate to high R_{max} . At RENO, the model presents negligible shifts in 2-year cycles of OC and NH_4
 529 while phase shifts of 0.3 and -0.5 cycles are simulated in the 3-year cycles for SO_4 and NH_4 . At ATL, the phase shift
 530 of -0.2 to -0.4 cycles are simulated for $PM_{2.5}$, NH_4 , OC, and EC with periods of 2- to 3-year cycles; while 2- to 3-year
 531 SO_4 cycles have a half-year cycle shift.

532 5 Conclusions

533 The main advantage for using EMD to evaluate PM_{2.5} and its speciated components is that it decomposes nonlinear
534 and nonstationary signals into multiple modes and a residual trend component. It does not require any preselection of
535 the temporal scales and assumptions of linearity and stationarity for the data, thereby providing insights into time
536 series of PM_{2.5} concentrations and its components. Using improved CEEMDAN, we are able to assess how well
537 regional-scale air quality models like CMAQ can simulate the intrinsic time-dependent long-term trend and cyclic
538 variations in daily average PM_{2.5} and its species. This type of coordinated decomposition and evaluation of total and
539 speciated PM_{2.5} provides a unique opportunity for modelers to assess influences of each PM_{2.5} species to the total
540 PM_{2.5} concentration in terms of time shifts for various temporal cycles and the magnitude of each component including
541 the trend.

542 A demonstration of how improved CEEMDAN could be applied to [PM_{2.5}](#) time series ~~data~~ at three sites over CONUS
543 that provide speciated PM_{2.5} data reveals the presence of the annual cycles in PM_{2.5} concentrations and time-
544 dependent features in all decomposed components. At these three sites, the model generally is more capable of
545 simulating the change rate in the trend component than the absolute magnitude of the long-term trend component.
546 However, the magnitude of SO₄ trend components is well represented across all three sites. Also, the model reproduced
547 the amplitude of the annual cycles for total PM_{2.5}, SO₄ and OC. The phase difference in the annual cycles for total
548 PM_{2.5}, OC and EC reveal a shift of up to half-year, indicating the need for proper allocation of emissions and an
549 updated treatment of organic aerosols compared to the earlier model version used in this set of model simulations. The
550 consistent large under/over-prediction of NO₃ variability at all temporal scales and magnitude in the trend component,
551 as well as the abnormally low correlations of synoptic scale NO₃ at ATL, calls for better representation of nitrate
552 partitioning and chemistry. Wildfires have the potential to elevate PM_{2.5} for months and can alter its variability at
553 scales from few days to the entire year. Thus, more accurate fire emission data should be incorporated to improve
554 model simulation, especially in those fire-prone regions.

555 **Data availability.** Paired observations and CMAQ model data used in the analysis will be made available at
556 <https://edg.epa.gov/metadata/catalog/main/home.page>. Raw CMAQ model outputs are available on request from the
557 U.S EPA authors.

558 **Author contribution.** "HL and MA designed the methodology; RM, CH and SR contributed in the assessment of the
559 outcomes and were consulted on necessary revisions. Model simulations were performed by the US EPA. HL prepared
560 the manuscript with contributions from all co-authors."

561 **Acknowledgements**

562 The views expressed in this paper are those of the authors and do not necessarily represent the view or policies of the
563 U.S. Environmental Protection Agency. Two of the authors (MA and HL) acknowledge that part of this work was
564 supported by the Electric Power Research Institute (EPRI) Contract #00-10005071, 2015–2017.

565 **References**

566 [Appel, K.W., Napelenok, S.L., Foley, K.M., Pye, H.O., Hogrefe, C., Luecken, D.J., Bash, J.O., Roselle, S.J., Pleim,](#)
567 [J.E., Foroutan, H. and Hutzell, W.T., 2017. Description and evaluation of the Community Multiscale Air Quality](#)
568 [\(CMAQ\) modeling system version 5.1. Geoscientific Model Development, 10\(4\), p.1703.](#)

569 Astitha, M., Luo, H., Rao, S.T., Hogrefe, C., Mathur, R., Kumar, N., [2017.](#) Dynamic evaluation of two decades of
570 WRF-CMAQ ozone simulations over the contiguous United States. *Atmospheric Environment* 164, 102–116.

571 Banzhaf, S., Schaap, M., Kraneburg, R., Manders, A.M.M., Segers, A.J., Visschedijk, A.H.J., Denier van der on,
572 H.A.C., Kuenen, J.P.P., van Meijgaard, E., van Ulft, L.H., Cofala, J., Builtjes, P.J.H., 2015. Dynamic model evaluation
573 for secondary inorganic aerosol and its precursors over Europe between 1990 and 2009. *Geoscientific Model*
574 *Development* 8, 1047–1070.

575 Chang, P.C., Flatau, A., Liu, S.C., 2003. Review Paper: Health Monitoring of Civil Infrastructure. *Structural Health*
576 *Monitoring* 2, 257–267.

577 Chen, X., Wu, Z., Huang, N.E., 2010. The time-dependent intrinsic correlation based on the empirical mode
578 decomposition. *Adv. Adapt. Data Anal.* 02, 233–265.

579 Civerolo, K., Hogrefe, C., Zalewsky, E., Hao, W., Sistla, G., Lynn, B., Rosenzweig, C., Kinney, P.L., 2010. Evaluation
580 of an 18-year CMAQ simulation: Seasonal variations and long-term temporal changes in sulfate and nitrate.
581 *Atmospheric Environment* 44, 3745–3752.

582 Colominas, M.A., Schlotthauer, G., Torres, M.E., 2014. Improved complete ensemble EMD: A suitable tool for
583 biomedical signal processing. *Biomedical Signal Processing and Control* 14, 19–29.

584 Derot, J., Schmitt, F.G., Gentilhomme, V., Morin, P., 2016. Correlation between long-term marine temperature time
585 series from the eastern and western English Channel: Scaling analysis using empirical mode decomposition. *Comptes*
586 *Rendus Geoscience* 348, 343–349.

587 Edgerton, E.S., Hartsell, B.E., Saylor, R.D., Jansen, J.J., Hansen, D.A., Hidy, G.M., 2005. The Southeastern Aerosol
588 Research and Characterization Study: Part II. Filter-Based Measurements of Fine and Coarse Particulate Matter Mass
589 and Composition. *Journal of the Air & Waste Management Association* 55, 1527–1542.

590 Foley, K.M., Hogrefe, C., Pouliot, G., Possiel, N., Roselle, S.J., Simon, H., Timin, B., 2015. Dynamic evaluation of
591 CMAQ part I: Separating the effects of changing emissions and changing meteorology on ozone levels between 2002
592 and 2005 in the eastern US. *Atmospheric Environment* 103, 247–255.

593 Gan, C.-M., Pleim, J., Mathur, R., Hogrefe, C., Long, C.N., Xing, J., Wong, D., Gilliam, R., Wei, C., 2015. Assessment
594 of long-term WRF-CMAQ simulations for understanding direct aerosol effects on radiation “brightening” in the
595 United States. *Atmospheric Chemistry and Physics* 15, 12193–12209.

596 [Gyawali, M., Arnott, W.P., Lewis, K. and Moosmüller, H., 2009. In situ aerosol optics in Reno, NV, USA during and](#)
597 [after the summer 2008 California wildfires and the influence of absorbing and non-absorbing organic coatings on](#)
598 [spectral light absorption. Atmospheric Chemistry & Physics, 9\(20\).](#)

599 Hansen, D.A., Edgerton, E.S., Hartsell, B.E., Jansen, J.J., Kandasamy, N., Hidy, G.M., Blanchard, C.L., 2003. The
600 Southeastern Aerosol Research and Characterization Study: Part 1—Overview. *Journal of the Air & Waste*
601 *Management Association* 53, 1460–1471.

602 He, J., Zhang, M., Chen, X., & Wang, M., 2014. Inter-comparison of seasonal variability and nonlinear trend between
603 AERONET aerosol optical depth and PM10 mass concentrations in Hong Kong. *Science China Earth*
604 *Sciences*, 57(11), 2606-2615.

605 Henneman, L.R.F., Liu, C., Hu, Y., Mulholland, J.A., Russell, A.G., 2017. Air quality modeling for accountability
606 research: Operational, dynamic, and diagnostic evaluation. *Atmospheric Environment* 166, 551–565.

607 Hogrefe, C., Hao, W., Zalewsky, E.E., Ku, J.-Y., Lynn, B., Rosenzweig, C., Schultz, M.G., Rast, S., Newchurch, M.J.,
608 Wang, L., Kinney, P.L., Sistla, G., 2011. An analysis of long-term regional-scale ozone simulations over the
609 Northeastern United States: variability and trends. *Atmospheric Chemistry and Physics* 11, 567–582.

610 Huang, N.E., Shen Zheng, Long Steven R., Wu Manli C., Shih Hsing H., Zheng Quanan, Yen Nai-Chyuan, Tung Chi
611 Chao, Liu Henry H., 1998. The empirical mode decomposition and the Hilbert spectrum for nonlinear and non-
612 stationary time series analysis. *Proceedings of the Royal Society of London. Series A: Mathematical, Physical and*
613 *Engineering Sciences* 454, 903–995.

614 Huang, Y., Schmitt, F.G., 2014. Time dependent intrinsic correlation analysis of temperature and dissolved oxygen
615 time series using empirical mode decomposition. *Journal of Marine Systems* 130, 90–100.

616 Kang, D., Hogrefe, C., Foley, K.L., Napelenok, S.L., Mathur, R., Trivikrama Rao, S., 2013. Application of the
617 Kolmogorov–Zurbenko filter and the decoupled direct 3D method for the dynamic evaluation of a regional air quality
618 model. *Atmospheric Environment* 80, 58–69.

619 Kelly, J.T., Koplitz, S.N., Baker, K.R., Holder, A.L., Pye, H.O.T., Murphy, B.N., Bash, J.O., Henderson, B.H., Possiel,
620 N.C., Simon, H., Eyth, A.M., Jang, C., Phillips, S., Timin, B., 2019. Assessing PM2.5 model performance for the
621 conterminous U.S. with comparison to model performance statistics from 2007-2015. *Atmospheric Environment* 214,
622 116872.

623 Mathur, R., Xing, J., Gilliam, R., Sarwar, G., Hogrefe, C., Pleim, J., Pouliot, G., Roselle, S., Spero, T.L., Wong, D.C.,
624 Young, J., 2017. Extending the Community Multiscale Air Quality (CMAQ) Modeling System to Hemispheric Scales:
625 Overview of Process Considerations and Initial Applications. *Atmos Chem Phys* 17, 12449–12474.

626 Moghtaderi, A., Borgnat, P., Flandrin, P., 2012. Gap-filling by the empirical mode decomposition, in: 2012 IEEE
627 International Conference on Acoustics, Speech and Signal Processing (ICASSP). Presented at the 2012 IEEE
628 International Conference on Acoustics, Speech and Signal Processing (ICASSP), pp. 3821–3824.

629 [Murphy, B.N., Woody, M.C., Jimenez, J.L., Carlton, A.M.G., Hayes, P.L., Liu, S., Ng, N.L., Russell, L.M., Setyan,](#)
630 [A., Xu, L. and Young, J., 2017. Semivolatile POA and parameterized total combustion SOA in CMAQv5. 2: impacts](#)
631 [on source strength and partitioning. Atmospheric Chemistry and Physics, 17, p.11107.](#)

632 Rato, R.T., Ortigueira, M.D., Batista, A.G., 2008. On the HHT, its problems, and some solutions. Mechanical Systems
633 and Signal Processing, Special Issue: Mechatronics 22, 1374–1394.

634 Torres, M.E., Colominas, M.A., Schlotthauer, G., Flandrin, P., 2011. A complete ensemble empirical mode
635 decomposition with adaptive noise, in: 2011 IEEE International Conference on Acoustics, Speech and Signal
636 Processing (ICASSP). Presented at the 2011 IEEE International Conference on Acoustics, Speech and Signal
637 Processing (ICASSP), pp. 4144–4147.

638 White, W.H., 2008. Chemical markers for sea salt in IMPROVE aerosol data. Atmospheric Environment 42, 261–
639 274.

640 Wong, D.C., Pleim, J., Mathur, R., Binkowski, F., Otte, T., Gilliam, R., Pouliot, G., Xiu, A., Young, J.O., Kang, D.,
641 2012. WRF-CMAQ two-way coupled system with aerosol feedback: software development and preliminary results.
642 Geoscientific Model Development 5, 299–312.

643 Wu, Z., Huang, N.E., 2004. A study of the characteristics of white noise using the empirical mode decomposition
644 method. Proceedings of the Royal Society of London. Series A: Mathematical, Physical and Engineering Sciences
645 460, 1597–1611.

646 Wu, Z., Huang, N.E., 2009. Ensemble empirical mode decomposition: a noise-assisted data analysis method. Adv.
647 Adapt. Data Anal. 01, 1–41.

648 Wu, Z., Huang, N.E., Long, S.R., Peng, C.-K., 2007. On the trend, detrending, and variability of nonlinear and
649 nonstationary time series. PNAS 104, 14889–14894.

650 Xing, J., Mathur, R., Pleim, J., Hogrefe, C., Gan, C.-M., Wong, D.C., Wei, C., Gilliam, R., Pouliot, G., 2015.
651 Observations and modeling of air quality trends over 1990–2010 across the Northern Hemisphere: China, the United
652 States and Europe. Atmospheric Chemistry and Physics 15, 2723–2747.

653 Xing, J., Pleim, J., Mathur, R., Pouliot, G., Hogrefe, C., Gan, C.-M., Wei, C., 2013. Historical gaseous and primary
654 aerosol emissions in the United States from 1990 to 2010. Atmospheric Chemistry and Physics 13, 7531–7549.

655 [Xu, L., Pye, H.O., He, J., Chen, Y., Murphy, B.N. and Ng, L.N., 2018. Experimental and model estimates of the](#)
656 [contributions from biogenic monoterpenes and sesquiterpenes to secondary organic aerosol in the southeastern United](#)
657 [States. Atmospheric chemistry and physics, 18\(17\), p.12613.](#)

658 Yahya, K., Wang, K., Campbell, P., Glotfelty, T., He, J., Zhang, Y., 2016. Decadal evaluation of regional climate, air
659 quality, and their interactions over the continental US using WRF/Chem version 3.6.1. Geoscientific Model
660 Development 9, 671–695.

- 661 Yeh, J.-R., Shieh, J.-S., Huang, N.E., 2010. Complementary ensemble empirical mode decomposition: a novel noise
662 enhanced data analysis method. *Adv. Adapt. Data Anal.* 02, 135–156.
- 663 Yu, L., Wang, S., Lai, K.K., 2008. Forecasting crude oil price with an EMD-based neural network ensemble learning
664 paradigm. *Energy Economics* 30, 2623–2635.
- 665 Zhou, W., Cohan, D.S., Napelenok, S.L., 2013. Reconciling NOx emissions reductions and ozone trends in the U.S.,
666 2002–2006. *Atmospheric Environment* 70, 236–244.
- 667